

ORIGINAL RESEARCH

Candesartan Cilexetil Attenuates Arrhythmogenicity Following Pressure Overload in Rats via the Modulation of Cardiac Electrical and Structural Remodeling and Calcium Handling Dysfunction

Gwo-Jyh Chang , PhD; Yung-Hsin Yeh, MD; Wei-Jan Chen, MD, PhD; Yu-Shien Ko, MD, PhD; Ying-Ju Lai, PhD; Yun-Shien Lee, PhD

BACKGROUND: Cardiac hypertrophy is associated with abnormal electrophysiology and increased arrhythmia risk. This study assessed whether candesartan cilexetil, an angiotensin II type 1 receptor blocker, could suppress arrhythmogenicity by attenuating cardiac electrical remodeling and calcium mishandling in rats with pressure-overload hypertrophy.

METHODS AND RESULTS: Male Sprague-Dawley rats were randomly subjected to abdominal aorta banding or sham procedure and received either candesartan cilexetil (3.0 mg/kg per day) or vehicle by gavage for 5 weeks. Pressure overload was characterized by compensated left ventricular (LV) hypertrophy and fibrosis, increased LV pressure and its decay time, and prolonged corrected QT interval, all of which were attenuated by candesartan cilexetil treatment. Candesartan cilexetil-treated banded rat hearts displayed shorter QT intervals and lower vulnerability to atrial and ventricular tachyarrhythmias than vehicle-treated banded hearts. Candesartan cilexetil prevented banding-induced prolonged action potential duration and reduced the occurrence of triggered activity in LV papillary muscles. In addition, the prolonged time to 50% cell relengthening and calcium transient decay time were normalized in LV myocytes from candesartan cilexetil-treated banded rats, along with a normalization of decreased SERCA2a (sarco[endo]plasmic reticulum calcium-ATPase) expression in LV tissues. Furthermore, candesartan cilexetil normalized depressed transient outward potassium current densities and protein and mRNA levels of both voltage-gated potassium 4.2 and 4.3 channel subunits (Kv4.2 and Kv4.3) in banded rats.

CONCLUSIONS: Candesartan cilexetil protects the heart from pressure overload-induced adverse electrical remodeling by preserving potassium channel densities. In addition, calcium handling and its molecular regulation also improved after treatment. These beneficial effects may contribute to a lower susceptibility to arrhythmias in hearts from candesartan cilexetil-treated pressure-overloaded rats.

Key Words: Ca²⁺ handling ■ candesartan cilexetil ■ cardiac electrical remodeling ■ ion channels ■ pressure overload

See Editorial by Salama

Cardiac hypertrophy is prevalent in a substantial portion of individuals with pressure or volume overload and is an independent risk factor of major cardiac events.^{1,2} Although the initial response is beneficial in normalizing wall stress and maintaining cardiac function, prolonged hypertrophy has

Correspondence to: Gwo-Jyh Chang, PhD, Graduate Institute of Clinical Medicinal Sciences, College of Medicine, Chang Gung University, 259 Wen-Hwa 1st Road, Kwei-Shan, Tao-Yuan 33302, Taiwan. Email: gjchang@mail.cgu.edu.tw

Supplemental Material for this article is available at <https://www.ahajournals.org/doi/suppl/10.1161/JAHA.121.024285>

For Sources of Funding and Disclosures, see page 22.

© 2022 The Authors. Published on behalf of the American Heart Association, Inc., by Wiley. This is an open access article under the terms of the [Creative Commons Attribution-NonCommercial-NoDerivs](#) License, which permits use and distribution in any medium, provided the original work is properly cited, the use is non-commercial and no modifications or adaptations are made.

JAHA is available at: www.ahajournals.org/journal/jaha

CLINICAL PERSPECTIVE

What Is New?

- Chronic treatment with candesartan cilexetil prevents pressure overload-induced adverse cardiac electrical remodeling mainly by preserving transient outward potassium current densities and channel expression.
- Candesartan cilexetil normalized the abnormal kinetics of cell shortening and calcium transient in hypertrophied ventricular myocytes mainly by protecting the downregulation of sarcoplasmic reticulum calcium pump SERCA2a (sarco[endo]plasmic reticulum calcium-ATPase) expression.
- Normalization of the structural and electrical abnormalities as well as calcium dysregulation by candesartan cilexetil contribute to a normal cardiac performance and a lower susceptibility to atrial and ventricular arrhythmias in pressure-overloaded rat hearts.

What Are the Clinical Implications?

- Prevention of left ventricular hypertrophy and electromechanical remodeling following pressure overload by candesartan cilexetil, an AT₁ receptor blocker with novel inverse agonist activity, but not by hydralazine, confirms that simply lowering blood pressure was insufficient to prevent cardiac remodeling.
- Clinical studies demonstrated the benefit of candesartan in preventing the progression of heart failure and thereby reducing the number of hospital admissions for chronic heart failure.
- Our results reinforce the idea that it is necessary to use antihypertensive drugs, with potent effects to prevent cardiac remodeling and rhythm disturbances, for treating hypertensives with cardiac hypertrophy or failure.

Nonstandard Abbreviations and Acronyms

AB	aortic banding
Ang II	angiotensin II
APD	action potential duration
$I_{Ca,L}$	L-type Ca ²⁺ current
I_{K1}	inward rectifier K ⁺ current
I_{Na}	peak Na ⁺ current
I_{SS}	steady-state outward K ⁺ current
I_{to}	transient outward K ⁺ current
KCHIP2	Kv-channel interacting protein 2
NCX	Na ⁺ -Ca ²⁺ exchanger
RyR2	ryanodine receptor Ca ²⁺ release channel 2
SERCA	sarco(endo)plasmic reticulum Ca ²⁺ -ATPase
SR	sarcoplasmic reticulum

deleterious consequences that lead to heart failure. The hypertrophied heart is associated with adaptive structural and electromechanical remodeling and is at greater risk of devastating arrhythmias and sudden death.^{3,4} The most consistent electrical change of the hypertrophied cardiomyocyte is prolonged action potential duration (APD),⁵ which may lead to an increased dispersion of refractoriness, thereby predisposing to arrhythmias.^{6,7} Decreased potassium (K⁺) currents, especially the transient outward K⁺ current (I_{to}), represents an early remodeling event in the hypertrophied myocardium.^{4,8,9} Additionally, defects in calcium (Ca²⁺) homeostasis contribute to both Ca²⁺-dependent hypertrophic signaling¹⁰ and disease-related electromechanical remodeling.⁵ Therefore, modulation of the pathophysiology of the electrical remodeling and Ca²⁺ mishandling are emerging as major upstream therapeutic targets for reducing arrhythmia risk.

Both mechanical stress and neurohumoral factors have been implicated in the development of cardiac hypertrophy during an increased hemodynamic load. In particular, angiotensin II (Ang II) plays a critical role in these pathophysiological processes. A significant amount of evidence has indicated that local Ang II synthesis is augmented by myocardial stretch,^{11,12} which might be of clinical relevance in the context of an increased workload. Further study has demonstrated that mechanical stretch can induce cardiac hypertrophy by activating Ang II type 1 (AT₁) receptors without involving Ang II.¹³ AT₁ receptor (AT₁R) blockers are a highly effective, well-tolerated class of drugs indicated for hypertension. Many clinical studies have shown that AT₁ receptor blockers help prevent the progression of heart failure, thereby reducing cardiac morbidity and mortality.^{14,15}

Candesartan is a more recently developed AT₁ receptor blocker, with noncompetitive antagonistic properties highly specific to AT₁ receptors. Candesartan possesses the highest affinity for AT₁ receptors among the AT₁ receptor blockers.¹⁶ It can also act as an inverse agonist that may stabilize the receptor in an inactive conformation and thus prevent its activation either by stretch or Ang II.¹³ Experimental studies have shown that candesartan can prevent or regress left ventricular (LV) hypertrophy in hypertensive^{17,18} or pressure-overloaded¹⁹ rats and reduce the stretch-induced hypertrophic response in cardiomyocytes.¹⁷ A recent study suggested that candesartan improved cardiac function in pressure-overloaded mice by suppressing matrix metalloproteinase-9-mediated cardiac structural remodeling.²⁰ The Candesartan in Heart Failure: Assessment of Reduction in Mortality and Morbidity (CHARM)-Preserved Trial revealed that candesartan prevents the number of hospital admissions for chronic heart failure.²¹ Further research suggests that candesartan reduced the incidence of new atrial fibrillation in a broad spectrum of patients with symptomatic

heart failure.²² An animal study also found that this agent improved arrhythmia morbidity in mice with pressure overload-induced LV hypertrophy.²³ The cardioprotective effects of candesartan have been extensively studied; however, the detailed cellular mechanism(s) of the antiarrhythmic effects remain largely unknown.

In the present study, we tested the hypothesis that the blockade of AT₁ receptors by candesartan cilexetil attenuates cardiac structural and electromechanical remodeling, as well as Ca²⁺ mishandling, and thereby suppresses induction of tachyarrhythmias in an aortic banding (AB)-induced, pressure-overloaded rat model.

METHODS

The data that support the findings of this study are available from the corresponding author upon reasonable request. All data, methods, and supporting materials have been provided within the article and Supplemental Material. An expanded Methods section is provided in Data S1.

Ethical Approval

All experiments were approved by the Institutional Animal Care and Use Committee of Chang Gung University (approval number: CGU06-41) and were performed in accordance with the *Guide for the Care and Use of Laboratory Animals* (National Research Council, Eighth Edition, 2011).

Animal Model of Aortic Banding-Induced Pressure Overload

Adult male Sprague-Dawley rats (BioLASCO, Taipei, Taiwan), weighing 190 to 220 g, were anesthetized by intraperitoneal injection of 30 mg/kg pentobarbital sodium. Under aseptic conditions, a midline laparotomy was performed, and the suprarenal abdominal aorta was looped with 3-0 silk suture. The suture was tightened around a 25-gauge needle (0.5 mm in diameter), which produced approximately 75% stenosis of the aortic diameter, and then the needle was withdrawn. Sham-operated rats underwent a similar surgical procedure without aorta constriction. Animals were randomly divided into the following groups: sham procedure receiving vehicle (Sham+Veh, n=32), sham procedure receiving candesartan cilexetil (Sham+Can, n=33), AB receiving vehicle (AB+Veh, n=34), and AB receiving candesartan cilexetil (AB+Can, n=34). In a separate study, banded rats were treated with hydralazine (AB+Hyd, n=23) for comparison. A total of 156 rats were used. No mortality or adverse events were observed in any animals in this study. A large number of animals were used for our study because we needed to perform diverse experiments following the in vivo study. Candesartan cilexetil (3.0 mg/kg per day, gavage) or

hydralazine (20 mg/kg per day, gavage) administration began the day after the surgery and continued for 5 weeks. The dosage regime for candesartan cilexetil was selected on the basis of previous literatures to be effective to reduce blood pressure moderately comparable to the extent of 20 mg/kg per day hydralazine. Candesartan cilexetil (kindly provided by AstraZeneca, Cambridge, United Kingdom) and hydralazine (Sigma-Aldrich, St. Louis, MO) were suspended in 2% gum Arabic solution. The control group was given the same volume of vehicle. All rats were housed in a constant-temperature and constant-humidity facility, exposed to a 12/12-hour light–dark cycle, and given standard rat chow and water. The rats were euthanized 5 weeks after the surgery. All treatments were withdrawn 24 hours before the experiments to eliminate the direct effect. All the experiments were performed by using male rats to avoid the influence of sex hormones.

In Vivo Hemodynamic and ECG Measurements

Rats were anesthetized with urethane (1.25 g/kg, IP) and tracheotomized to facilitate breathing. Femoral arterial pressure was measured using a polyethylene (polyethylene 50) cannula. The arterial cannula was connected to a pressure transducer (MLT0380/D; ADInstruments, Sydney, Australia), and the signal was amplified by a QuadBridge amplifier (ADInstruments). Lead II ECGs were recorded using subdermal needle electrodes. To measure LV pressure and volume, a 1.9-French microtip pressure–volume (P–V) catheter (Scisense, London, ON, Canada) was inserted from the right carotid artery and advanced into the left ventricle under pressure control. The signals were continuously recorded at a sampling rate of 4 kHz using a P–V conductance system (model 896B; Scisense). Output signals were connected to an acquisition system (ACQ16; DSI Ponemah, St. Paul, MN) and were computed using a cardiac P–V analysis program (P3 Plus4.80-SP4; DSI Ponemah). P–V relations were measured by transiently compressing the inferior vena cava. These measures include the slopes of end-systolic and end-diastolic P–V relations, the slope of preload recruitable stroke work, defined as the relationship between stroke work and end-diastolic volume, where stroke work is the P–V loop area for each beat. After the hemodynamic recordings, the rats were euthanized under deep anesthesia, and their hearts were quickly excised for performing the subsequent diverse experiments.

Determination of Ang II Levels of Serum and Left Ventricular Samples via ELISA

After the hemodynamic recordings, blood samples were obtained from the arterial polyethylene catheter

and centrifuged at 4 °C. Protein samples were extracted from the LV tissues as described below in the Western blot analysis subsection. Ang II levels were measured using an ELISA assay kit (CSB-E04494r; CUSABIO, Houston, TX) according to the manufacturer's instructions. Eight-point standard curves were obtained for each test using known concentrations with optical densities plotted against concentrations. Ang II levels in LV tissues were normalized for total protein content, measured in the same samples.

Histological Analysis

Isolated hearts were fixed with 10% formalin in phosphate-buffered saline and embedded in paraffin. Hearts were cut transversely in the middle of the ventricle. Several ventricular and left atrial sections (5- μ m thick) were prepared and stained with hematoxylin and eosin to assess the overall morphology. The extent of cardiac fibrosis was examined using Masson's trichrome staining. The fraction of interstitial fibrosis area was quantified on 5 fields per slice for each heart by use of Image-Pro Premier 9.0 (Media Cybernetics, Rockville, MD).

Ex Vivo Intracardiac Electrogram Recording of Langendorff-Perfused Hearts

Each explanted heart was mounted on Langendorff perfusion apparatus and retrogradely perfused at a rate of 6 mL/min per gram of cardiac tissue with oxygenated (95% O₂ and 5% CO₂) normal Tyrode's solution (composition [millimole per Liter]: 137 NaCl, 5.4 KCl, 1.1 MgCl₂, 11.9 NaHCO₃, 0.33 NaH₂PO₄, 1.8 CaCl₂, and 11 dextrose) at 37 °C, as described previously.²⁴ A 1.2-French octapolar electrophysiology catheter (Scisense) was used to record the His-bundle electrogram, whereas the other platinum electrode was placed on the ventricular apex to record epicardial ventricular electrograms. To pace the atrium and ventricle, one pacing electrode was placed on the right atrium and the second was placed on the right ventricular apex. Pacing stimuli (1-millisecond duration, twice-threshold voltage) were delivered by a programmable stimulator (DTU 215; Fischer Imaging, Denver, CO). The signals were continuously monitored and recorded on a chart recorder (WindowGraf; Gould, Cleveland, OH), and digitized simultaneously with a computer-based data acquisition system (IWX/214; iWorx, Dover, NH). Electrophysiological studies were performed according to standard methods described previously.²⁴ The average of 4 stable cycle lengths of spontaneous heartbeats was taken as the pacemaker automaticity. The right atrium was then paced at a constant rate that was slightly faster than the spontaneous heart rate. At this constant rate pacing, the intra-atrial

(stimulus-atrial conduction interval), atrioventricular (AV) nodal (atrio-His bundle conduction interval), and His-ventricular conduction intervals, and QT interval were measured. Incremental right atrial pacing was used to determine the Wenckebach cycle length, at which the 1:1 atrioventricular conduction was lost. Atrial premature extrastimulation (S₂) after a train of constant rate atrial pacing (S₁S₁) for 8 beats was then performed to obtain the refractory periods of the atria, atrioventricular node, and His-Purkinje system. The ventricular effective refractory period was determined using a ventricular extrastimulation study protocol.

Atrial Tachyarrhythmia Vulnerability in Ex Vivo Perfused Hearts

A bipolar electrode was placed on the left atrium to record the atrial electrogram. Pacing current was delivered via a bipolar electrode placed on the right atrial appendage. The interatrial conduction time was defined as the time from the right atrial (RA) appendage pacing spike to the left atrial appendage activation at a pacing cycle length of 200 milliseconds. Atrial tachyarrhythmia (AT) was induced with burst pacing after 8 regularly paced stimuli (S₁) at a 200-millisecond pacing cycle length and 5-fold diastolic threshold. The burst pacing current (S₂) consisted of a train of 100 square-wave pulses (1 millisecond in duration) at a frequency of 100 Hz for a duration of 1 second. The duration of AT was defined as a period of rapid irregular atrial rhythm deviating from sinus rhythm for >0.1 second. The mean duration of AT in each heart was determined on the basis of 5 inductions.

Ventricular Tachyarrhythmia Vulnerability in Ex Vivo Perfused Hearts

Ventricular epicardial electrograms were recorded by a bipolar electrode, placed on the epicardial surface of the LV apex. A bipolar pacing electrode was placed on the anterior epicardial surface of the right ventricle. Ventricular tachyarrhythmia induction was then attempted by programmed stimulation on the right ventricle at a pacing cycle length of 150 milliseconds (S₁) with 1 to 3 (S₂, S₃, and S₄) extrastimuli delivered after 8 regularly paced beats. The stimulation intensity was twice the threshold and 5 milliseconds in duration. Pacing protocols were interrupted if sustained ventricular tachyarrhythmia was induced. The testing end point was inducing nondriven ventricular tachyarrhythmias. A preparation was considered noninducible when ventricular pacing produced either no ventricular premature beats or only self-terminating salvos of <6 beats. Ventricular tachyarrhythmias, including ventricular tachycardia and fibrillation, were considered non-sustained when they lasted \leq 15 beats and sustained when they lasted >15 beats. An arrhythmia scoring

system was used, as previously described,²⁴ and is provided in Data S1.

Electrical Recordings in Isolated Cardiac Tissues

The LV papillary muscle (1–1.5 mm in diameter and 5–8 mm in length), left atrial (LA) strip, or LV free wall slice (0.2 mm in thickness) was dissected free and mounted in a tissue chamber, then superfused at a rate of 20 mL/min with an oxygenated normal Tyrode's solution at 37 °C.²⁴ The preparations were stimulated with 1-millisecond 1.5-fold threshold strength pulses through platinum field electrodes. Transmembrane potentials were recorded with a glass microelectrode filled with 3 mol/L KCl (tip resistance: 15–25 MΩ), which was connected to the input stage of an Axoclamp 2B amplifier (Molecular Devices, Sunnyvale, CA). Action potentials were digitized at 10 kHz by a PowerLab/4sp digitizer via Chart 5.0 software (ADInstruments) for off-line analysis.

Detection of Superoxide Anion Production by Chemiluminescence in Myocardial Tissues

Superoxide anion production in fresh LV or LA tissues (approximately 2 mg) was measured by lucigenin-enhanced chemiluminescence using a microplate luminometer (Plate CHAMELEON; Hidex, Turku, Finland), as previously described.²⁴ Photon outputs were measured after addition of lucigenin (5 μmol/L) and NADPH (100 μmol/L). Data were recorded from 5 tissues for each heart and normalized to the dry weight of tissues.

Western Blot Analysis

Frozen LV tissues were homogenized in ice-cold lysis buffer. Protein concentration was measured using a Protein Assay Reagent (Bio-Rad Laboratories, Hercules, CA) and adjusted for equal loading. Protein samples (30–100 μg) were separated on 4% to 20% gradient gel (Mini-Protean Precast gels; Bio-Rad Laboratories) or 8% to 10% SDS-PAGE and transferred onto polyvinylidene difluoride (PVDF) membranes (PerkinElmer Life Sciences, Boston, MA). Membranes were blocked and then incubated overnight at 4 °C with primary antibody against ryanodine receptor Ca²⁺ release channel 2 (RyR2) (1:1000; ThermoFisher Scientific, Waltham, MA), Ser²⁸⁰⁸-phosphorylated RyR2 (pSer²⁸⁰⁸-RyR2) (1:5000; Badrilla, Leeds, United Kingdom), pSer²⁸¹⁴-RyR2 (1:500; Badrilla), SERCA2a (sarco[endo]plasmic reticulum Ca²⁺-ATPase) (1:5000; Badrilla), phospholamban (1:2000; Badrilla), pSer¹⁶-phospholamban (1:2000; Millipore, Temecula, CA), pThr¹⁷-phospholamban (1:2000; Badrilla), Na⁺-Ca²⁺ exchanger 1 (NCX1) (1:500; Santa Cruz Biotechnology, Santa Cruz, CA), voltage-gated L-type calcium 1.2a channel subunit (Ca_v1.2a) (1:400;

Millipore), voltage-gated sodium 1.5 channel subunit (Na_v1.5) (1:500; Alomone, Jerusalem, Israel), voltage-gated potassium 4.2 channel subunit (Kv4.2) (1:200; Millipore), voltage-gated potassium 4.3 channel subunit (Kv4.3) (1:200; Alomone), voltage-gated potassium 1.4 channel subunit (Kv1.4) (1:200; Alomone), Kv-channel interacting protein 2 (KChIP2) (1:500; ThermoFisher Scientific), voltage-gated potassium 2.1 channel subunit (Kv2.1) (1:500; Alomone), and inwardly rectifying potassium 2.1 channel subunit (Kir2.1) (1:600; Alomone). The blot was also probed by a glyceraldehyde 3-phosphate dehydrogenase (GAPDH) antibody (1:1000; Santa Cruz) or a β-actin antibody (1:1000; Abcam, Cambridge, MA) as an internal control. The membranes were then incubated with horseradish peroxidase-tagged anti-mouse IgG (immunoglobulin G) (1:5000, Millipore) or anti-rabbit IgG (1:10000, Jackson ImmunoResearch, West Grove, PA) for 1 hour at room temperature. The antibody-antigen complexes in all membranes were detected by the enhanced chemiluminescence detection kit (PerkinElmer) according to the manufacturer's instructions and digitized in a BioSpectrum 500 Imaging System (UVP, Upland, CA). The densities of the immunoreactive bands were quantified using VisionWorks LS image software (version 6.6a; UVP). Additional details are provided in Data S1.

Real-Time Quantitative Reverse Transcription-Polymerase Chain Reaction

The total RNA samples were extracted from LV tissues using TRIzol reagent (Life Technologies, Rockville, MD). Gene expression levels were determined by real-time quantitative reverse transcription-polymerase chain reaction (ABI QuantStudio 12K Flex; ThermoFisher Scientific), as reported previously.²⁵ GAPDH mRNA was used as an internal control. The specific primers (Sigma-Aldrich) used were listed as follows: Kv4.2 (Kcnd2): forward: 5'-ATCAGATGTGTGGAGAGAAC-3' and reverse: 5'-TAATTATTGCTGTGGTCACG-3'; Kv4.3 (Kcnd3): forward: 5'-CAAAGTCAAAACACAAGAC-3' and reverse: 5'-GTGGAGAAAAACATTTTCACG-3'; GAPDH: forward: 5'-TCCCATTCTTCCACCTTT-3' and reverse: 5'-TAGCCATATTCATTGTCATACC-3'. Relative expressions of Kv4.2 and Kv4.3 were calculated using a 2^{-ΔΔct} method by SYBR green detection mechanism.

Measurements of Ca²⁺ Transients and Cell Shortening

Single ventricular cells were obtained by an enzymatic dissociation method described previously.²⁴ Intracellular Ca²⁺ transients were measured by fura-2 fluorescence at room temperature (25 °C–27 °C), as described previously.²⁴ Cytosolic loading of fura-2 was achieved by incubating cardiomyocytes with 5 μmol/L fura-2-AM and 2% Pluronic F-127 for 30 minutes at room temperature. After

washing out the excess dye, the loaded myocytes were transferred to 1.8 mmol/L Ca^{2+} containing HEPES buffer (composition [millimole per Liter]: NaCl 137.0, KCl 5.4, KH_2PO_4 1.2, MgSO_4 1.22, CaCl_2 1.8, dextrose 11.0, and HEPES 6.0, adjusted to pH 7.4 with NaOH) for at least 30 minutes. Fura-2-loaded myocytes were placed on an inverted microscope (Axio Observer Z1; Carl Zeiss, Jena, Germany) and were stimulated at 1 Hz by 2-millisecond square-wave pulses, with a voltage intensity of ~30% to 40% above the threshold. The cells were illuminated with ultraviolet light from a light source (DeltaScan; PTI-HORIBA Scientific, Edison, NJ). The excitation lights with a wavelength of 340 or 380 nm passed through a $\times 40$ oil immersion objective to the cell by a dichroic mirror. The emission light was collected at 510 nm by a photomultiplier tube and recorded with the RatioMaster fluorometer (PTI-HORIBA Scientific). The signals were acquired using a BriteBox data acquisition system controlled with Felix32 software (PTI-HORIBA Scientific). The ratio of the background-subtracted fluorescence signal (F_{340}/F_{380}) was used as the $[\text{Ca}^{2+}]_i$ index. Cell-shortening was measured optically with a video edge-detection system (R12; Crescent Electronics, Sandy, UT) simultaneously with fura-2 fluorescence. All signals were collected at a sampling rate of 200 points/s. Caffeine-induced Ca^{2+} transients were evoked by rapid bath application of 10 mmol/L caffeine on myocytes 10 seconds after stopping field stimulations of the myocytes with electrical pulses (for 20 seconds at 1-Hz stimulation frequency) to ensure stable sarcoplasmic reticulum (SR) Ca^{2+} load.

Whole-Cell Patch-Clamp Recording

Ionic currents were studied in whole-cell configuration at room temperature (25 °C–27 °C), as described previously.²⁴ A small aliquot of the solution containing the isolated cardiomyocytes was placed in a 1-mL chamber mounted on the stage of an inverted microscope (Axio Observer Z1; Carl Zeiss). Cells were bathed in 1.8 mmol/L Ca^{2+} HEPES-buffered Tyrode solution. Patch electrodes were fabricated from glass capillaries (OD: 1.5 mm, ID: 1.0 mm; A-M Systems, Carlsborg, WA) and fire-polished to give a pipette resistance of 2 to 5 M Ω when filled with the pipette solution and immersed in the external solution. Membrane currents were recorded using an integrating patch-clamp amplifier (Axopatch 200B; Molecular Devices). Command pulses were generated by a 16-bit Digidata 1320A D/A converter (Molecular Devices) controlled by pCLAMP8.0.2 software (Molecular Devices). Data acquisition and analyses were performed using the Clampex and Clampfit module of pCLAMP software, respectively. Recordings were filtered at 10 kHz and acquired at 100 kHz; they were stored on the hard disk of a computer for subsequent analysis. Electrode junction potentials (5–10 mV) were measured and nulled before suction of the cell. A high resistance seal (5–10 G Ω) was obtained before the disruption of the membrane patch.

After forming the whole-cell recording configuration, a capacitive transient induced by a 10-mV step from a holding voltage of 0 mV was recorded and used for the calculation of cell capacitance. Series resistance was in the 4- to 6-M Ω range and compensated by 60% to 80%. The average capacitance of the LV myocytes isolated from banded rats was significantly larger than that from sham controls (Sham+Veh: 205.5 \pm 40.1 pF, n=38 cells/9 rats; AB+Veh: 318.8 \pm 85.2 pF, n=39 cells/9 rats, $P<0.001$ by linear mixed model analysis), consistent with an increase in myocyte size. Treatment with candesartan cilexetil significantly reduced cell capacitance in AB rats (253.6 \pm 40.4 pF, n=36 cells/9 rats, $P<0.001$ versus AB+Veh group by linear mixed model analysis) with no change on sham control animals (228.7 \pm 56.7 pF, n=35 cells/9 rats; $P>0.05$ versus Sham+Veh).

To measure K^+ currents, pipettes were filled with normal K^+ containing internal solution (millimole per Liter): KCl 120, NaCl 10, MgATP 5, EGTA 5, and HEPES 10, and pH 7.2 titrated with KOH. During measurement of K^+ currents, Na^+ and Ca^{2+} inward currents were blocked by addition of 30 μM tetrodotoxin and 1 mmol/L CoCl_2 to the bathing solution, respectively. To measure Ca^{2+} inward current, the K^+ currents were blocked by adding CsCl (2 mmol/L) to the bathing medium and internal dialysis of the cells with Cs^+ and tetraethylammonium chloride-containing pipette solution (in millimole per Liter): CsCl 130.0, EGTA 5.0, tetraethylammonium (TEA) chloride 15.0, dextrose 5.0, and HEPES 10.0, adjusted to pH 7.2 with CsOH. For recording Na^+ inward current, the cells were dialyzed with Cs^+ and tetraethylammonium-containing pipette solution, and a K^+ -free bathing solution was used as follows (in millimole per Liter): NaCl 50.0, CsCl 90.0, MgCl_2 1.2, CaCl_2 1.0, CoCl_2 1.0, tetraethylammonium chloride 10.0, dextrose 11.0, and HEPES 5.0, adjusted to pH 7.4 with CsOH. Additional details are provided in Data S1.

Chemicals

All chemicals used were purchased from Sigma-Aldrich except for fura-2-AM and Pluronic F127, which were purchased from Molecular Probes (Eugene, OR). Fura-2-AM and Pluronic F127 were dissolved in dimethylsulfoxide. Other drugs were dissolved in physiological saline before the start of the experiment.

Statistical Analysis

Except for arrhythmia and triggered activity incidences, all data are expressed as mean \pm SD. Statistical analysis was performed using 1-way or 2-way ANOVA followed by post hoc Tukey test for multiple comparisons, where appropriate. For comparison of arrhythmia and triggered activity incidences between different groups, a 2 \times 2 contingency table using a Fisher exact test was used. To take into account repeated sample assessments, data with multiple cardiomyocytes acquired from

the same rat were analyzed with a linear mixed model. Statistical methods are described in each figure legend and table note. All statistical analyses were performed with SPSS Statistics (version 22.0; IBM, Armonk, NY). *P* values of <0.05 were considered statistically significant.

RESULTS

Candesartan Cilexetil Prevents Cardiac Hypertrophic Remodeling and Fibrosis

After 5 weeks of AB, the rats' hearts were globally enlarged. Cardiac hypertrophy was quantified by increased heart-to-body weight, left ventricle-to-body weight, and left atrium-to-body weight ratios (Table 1). Histological analysis showed that the cross-sectional diameters of both LV and LA myocytes were markedly increased in banded rats compared with sham controls (Figure S1). The above data suggest that compensatory concentric hypertrophy developed at 5 weeks of AB. All of these parameters were normalized by treatment with candesartan cilexetil. Although the nonspecific vasodilator hydralazine significantly decreased blood pressure in banded rats (see below), it did not prevent cardiac hypertrophy (Table 1). AB also caused moderate interstitial collagen deposition in both LV and LA free walls, as demonstrated by Masson's trichrome staining (Figure S2). Treatment with candesartan cilexetil further reduced myocardial fibrosis relative to the outcomes in untreated banded rat hearts. We next examined the Ang II levels in serum and LV free wall samples from various group rats. Serum levels of Ang II in vehicle-treated sham-operated and banded rats and in candesartan cilexetil-treated sham-operated and banded rats were 0.70 ± 0.82 , 2.06 ± 1.56 , 1.19 ± 0.64 , and 2.98 ± 2.27 pg/mL ($n=6$ each, *P*=not significant by 1-way ANOVA), respectively, whereas the levels in LV tissues from the corresponding groups were 43.8 ± 14.7 , 33.3 ± 7.1 , 37.5 ± 7.1 , and 41.0 ± 21.1 pg/mg protein ($n=6$ each, *P*=not significant by 1-way ANOVA). No significant differences were detected among the 4 groups.

Candesartan Cilexetil Prevents Changes in Ventricular Function and ECG Variables

Banded rats displayed increased LV end-systolic pressure and developed pressure and exhibited a tendency toward larger values of the maximal velocity of contraction, LV end-diastolic and end-systolic volume, and arterial elastance (index of ventricular afterload) (Table 1). These results suggest an increased cardiac load and that the LV chamber was slightly dilated in banded rats. Furthermore, LV end-diastolic pressure and the relaxation time constant (τ) increased significantly in banded rats, indicating diastolic dysfunction. The QRS, QT, and corrected QT intervals were also significantly longer in the banded group than in the sham controls (Figure 1A and Table 1). AB did not affect the femoral mean arterial pressure compared with

sham controls. Treatment of banded rats with candesartan cilexetil resulted in a modest reduction in mean arterial pressure, effectively to the same extent as that seen in the hydralazine-treated group. Candesartan cilexetil significantly prevented the banding-induced compensatory changes in LV function and prolongation of corrected QT interval, whereas hydralazine did not (Table 1).

We also determined other P–V loop–derived loading-independent indexes of LV systolic performance, such as end-systolic P–V relation and slope of preload recruitable stroke work, at different preloads. Slope of preload recruitable stroke work has been described as a highly linear, load-insensitive contractility measure. Figure 1B displays typical P–V loops obtained after inferior vena cava occlusions. End-systolic P–V relation and slope of preload recruitable stroke work were significantly higher in banded animals and were markedly normalized by treatment with candesartan cilexetil but not hydralazine (Figure 1C and 1E). The end-diastolic P–V relation, an index of LV stiffness, was similar in all enrolled animals (Figure 1D).

Intracardiac Electrograms of Langendorff-Perfused Hearts

An example array of intracardiac electrograms from different groups is shown in Figure 1F. The most significant changes in the conduction parameters of banded rat hearts were prolonged of QT interval and ventricular effective refractory period (Table 2). Candesartan cilexetil administration significantly prevented the prolongation of both the QT interval and ventricular effective refractory period in hearts from banded rats, whereas hydralazine did not. Other parameters showed no significant difference among all groups.

Candesartan Cilexetil Attenuates the Inducibility of Atrial and Ventricular Tachyarrhythmias

The inducibility of ATs in perfused hearts from each group was examined using a burst pacing protocol. Only a small number of ATs were induced in the sham control hearts. In contrast, a much higher inducibility and longer duration of AT were observed in the banded-group hearts (Figure 2A through 2C). Furthermore, the interatrial conduction time was significantly longer in the banded group than in the controls (Figure 2A and 2D). Candesartan cilexetil administration in the banded rats significantly reduced both the AT inducibility and duration, with normalization to interatrial conduction time.

Representative recordings of the ventricular tachyarrhythmias inductions by programmed electrical stimulation are shown in Figure 2E. The arrhythmia score in the sham control group, either with or without candesartan cilexetil treatment, was low (Figure 2F). In

Table 1. Physiological, Hemodynamic, Cardiac Performance, and ECG Variables Recorded 5 Weeks of Treatment From Various Group Rats

	Sham+Veh	AB+Veh	Sham+Can	AB+Can	AB+Hyd
No. of rats	17	19	17	19	16
Body weight, g	381±35	373±57	390±41	373±30	373±47
LAW/BW, mg/g	0.12±0.02	0.18±0.05 [#]	0.13±0.03	0.15±0.03 [†]	0.17±0.02 ^{**}
RVW/BW, mg/g	0.60±0.10	0.80±0.16 [#]	0.69±0.12	0.69±0.13	0.82±0.14 [#]
LVW/BW, mg/g	1.67±0.19	2.68±0.44 [#]	1.67±0.24	2.05±0.28 ^{**} , [§]	2.50±0.43 [#]
HW/BW, mg/g	3.37±0.30	5.08±0.87 [#]	3.47±0.41	4.00±0.54 [*] , [§]	4.78±0.64 [#]
Lung/BW, mg/g	4.89±0.97	5.22±1.09	5.04±0.90	4.74±0.43	4.97±0.81
No. of rats	32	34	33	34	23
HR, bpm	319±53	322±65	307±47	294±64	302±44
MAP, mm Hg	74.5±12.0	81.0±20.1	58.9±11.4 [#]	63.3±16.0 ^{*,§}	65.0±11.0 [‡]
LVESP, mm Hg	114.6±11.4	151.2±23.3 [#]	100.3±9.0 ^{**}	124.9±14.8 [§]	139.1±21.1 [#]
LVEDP, mm Hg	4.6±3.2	9.0±3.4 [#]	5.5±2.8	5.3±3.4 [§]	8.9±1.6 [#]
LVDP, mm Hg	110.0±11.0	142.3±22.8 [#]	94.7±8.0 ^{**}	119.7±14.4 [§]	130.2±20.6 [#]
dP/dt _{max} , mm Hg/s	8473±2235	9456±3071	7359±1914	8410±2039	8824±1722
dP/dt _{min} , mm Hg/s	5490±851	6035±1177	4948±1199	5762±1029	5707±761
τ, ms	8.8±3.5	12.5±2.8 [#]	9.4±2.9	9.4±2.7 [§]	11.6±2.3 ^{**}
V _{ES} , μL	78.1±36.5	107.0±45.3 [†]	82.7±28.4	86.6±40.4	93.9±25.4
V _{ED} , μL	157.0±56.2	196.4±61.8	154.1±59.5	174.8±65.9	205.2±49.8 [†]
EF, %	55.9±12.2	54.0±9.6	57.2±12.2	58.1±12.2	57.3±8.1
Ea, mm Hg/μL	1.21±0.60	1.56±0.66	1.18±0.86	1.28±0.67	1.14±0.35
PR, ms	62.0±9.0	60.8±8.1	59.5±7.5	61.1±6.7	57.7±6.7
QRS, ms	15.4±2.0	17.0±2.4 ^{**}	15.2±1.7	16.7±2.3	16.8±1.9
QT, ms	94.1±11.7	108.1±13.3 [#]	94.4±11.4	97.1±14.6	104.8±14.0 [†]
QTc, ms	216.0±26.9	247.0±20.2 [#]	212.5±29.5	218.0±31.7 [§]	237.0±36.4

Data are presented as mean±SD. AB indicates aortic banding; BW, body weight; Can, candesartan cilexetil; dP/dt_{max} and dP/dt_{min}, maximal rate of rise and decline of LV pressure; Ea, arterial elastance; EF, ejection fraction; HR, heart rate; HW, heart weight; Hyd, hydralazine; LAW, left atrial weight; LVDP, left ventricular developed pressure; LVEDP, left ventricular end-diastolic pressure; LVESP, left ventricular end-systolic pressure; LVW, left ventricular weight; MAP, mean arterial pressure; PR, PR interval of ECG; QRS, QRS duration of ECG; QT, QT interval of ECG; QTc, corrected QT interval, QT interval (in milliseconds) divided by the square root of RR interval (in seconds); RW, right ventricular weight; τ, time constant of left ventricular pressure decay; Veh, vehicle; and V_{ES} and V_{ED}, end-systolic and end-diastolic volume of the left ventricle.

[#]P<0.001 vs Sham+Veh group.

^{*}P<0.05 vs Sham+Veh group.

^{**}P<0.01 vs Sham+Veh group.

[§]P<0.001 vs AB+Veh group.

[†]P<0.05 vs AB+Veh group.

[‡]P<0.01 vs AB+Veh group by 1-way ANOVA with a Tukey post hoc test.

contrast, arrhythmia inducibility was significantly enhanced in the banded group compared with the sham controls, whereas it was significantly reduced with candesartan cilexetil treatment.

Candesartan Cilexetil Prevents the Prolongation of Ventricular Action Potential

Representative action potentials of LV papillary muscles driven at 1 and 4 Hz from each group are shown in Figure 3A. The APD at the 25%, 50%, and 90% repolarization levels were markedly prolonged at all frequencies (0.5–4 Hz) in the banded group compared with the sham controls (Figure 3B through 3D). The APD₉₀ restitution curve slope was significantly steeper in the banded group treated with vehicle (P<0.05

versus sham+vehicle group). The maximal upstroke velocity tended to be lower in the banded group than sham group, but this change did not reach statistical significance (Figure 3E). The prolonged APDs were significantly attenuated, and the reduced maximal upstroke velocity was normalized in the banded group by candesartan cilexetil but not by hydralazine treatment (Figure 3B through 3E). The steep APD₉₀ restitution curve in banded rats tended to be normalized by candesartan cilexetil but not by hydralazine. There were no significant differences in the other parameters among all groups (Figure 3F and 3G). In contrast, AB or candesartan cilexetil treatment was not associated with any change in AP parameters in LA strips (Figure S3). We further examined the regional differences of APD in LV free wall slices (Figure S4A). Our results showed that the LV free walls from sham

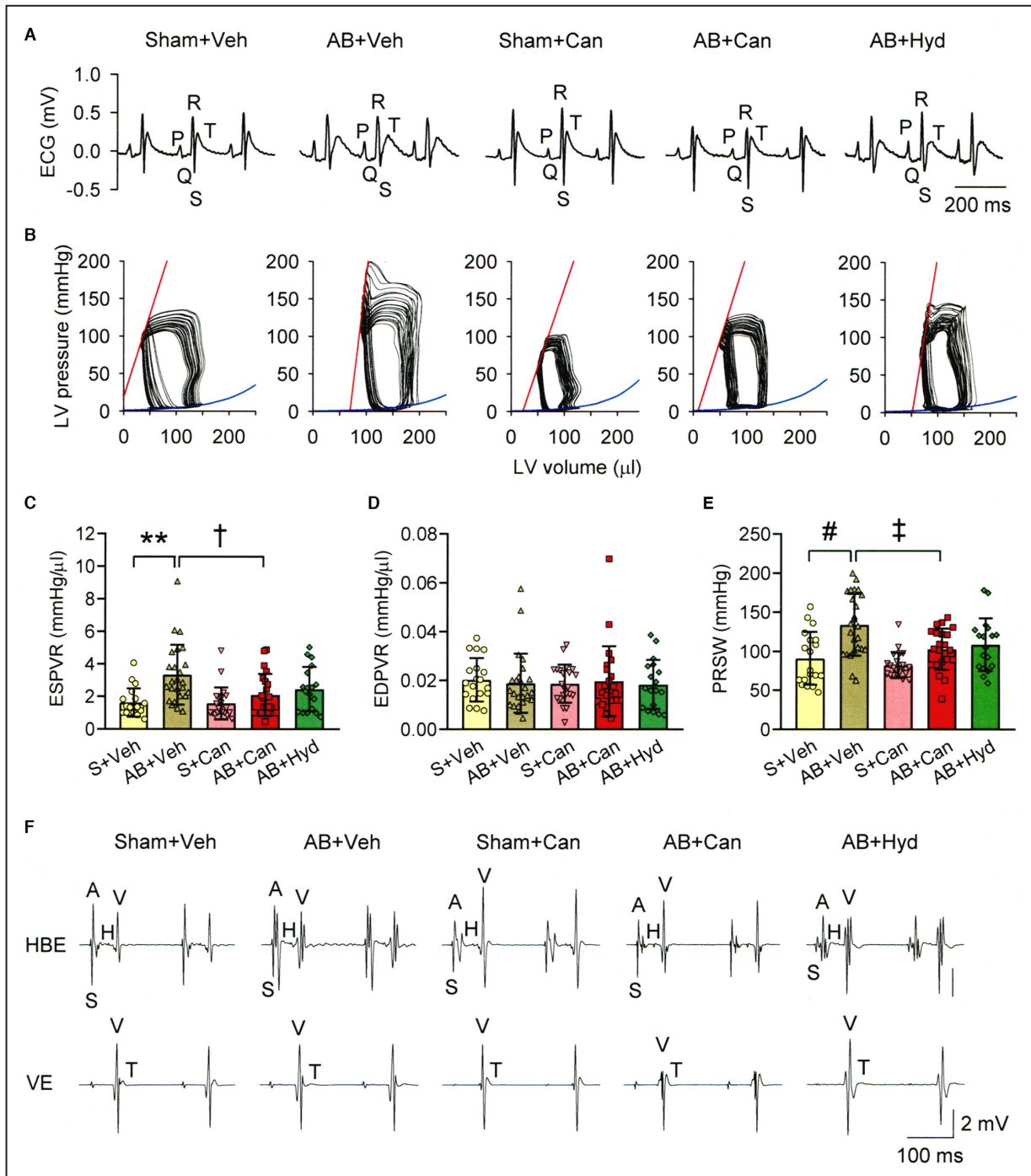


Figure 1. In vivo ECG and left ventricular pressure–volume (P–V) loop recordings in anesthetized rats and ex vivo intracardiac conduction electrogram recordings in perfused hearts.

A, Representative tracings of ECGs recorded in anesthetized rats from the 5 study groups: Sham+vehicle (Veh), aortic banding (AB)+Veh, Sham+candesartan cilexetil (Can), AB+Can, and AB+hydralazine (Hyd). **B–E**, In vivo heart function as shown by P–V relations in the 5 study groups. **B**, Representative P–V loops obtained at different preloads. End-systolic P–V relation (ESPVR; red lines) and end-diastolic P–V relation (EDPVR; blue lines) were calculated using a computerized algorithm. **C–E**, Load-independent contractile parameters measured as ESPVR (**C**) and preload recruitable stroke work (PRSW) (**E**) for systolic function and EDPVR (**D**) for diastolic stiffness in Sham+Veh (n=19), AB+Veh (n=25), Sham+Can (n=22), AB+Can (n=22), and AB+Hyd (n=17) rats. Values are presented as mean±SD. ***P*<0.01 and †*P*<0.001 vs Sham+Veh group; ‡*P*<0.05 and #*P*<0.01 vs AB+Veh group by 1-way ANOVA with a Tukey post hoc test. **F**, Representative His-bundle (HBE; upper) and ventricular electrograms (VE; lower) at a paced rhythm (200-milliseconds cycle length) of the Langendorff-perfused hearts from various groups. A indicates atrial depolarization; H, His-bundle depolarization; S, stimulation artifact; T, ventricular repolarization; and V, ventricular depolarization.

Table 2. Conduction System Parameters Recorded From the Isolated Perfused Hearts of Various Group Rats

	Sham+Veh, n=17	AB+Sham, n=19	Sham+Can, n=17	AB+Can, n=19	AB+Hyd, n=16
BCL	240.9±26.1	254.2±39.9	235.7±35.8	248.2±34.9	263.8±32.7
SA	10.2±1.9	9.7±0.7	9.8±0.6	9.7±0.7	10.2±1.3
AH	28.0±7.8	27.7±6.4	26.3±6.0	25.2±4.3	25.5±5.2
HV	18.2±2.9	20.5±5.6	19.7±2.7	19.7±4.1	18.1±3.5
QT	38.2±12.6	51.6±11.4*	40.3±15.4	41.6±9.9 [†]	55.6±8.1**
WCL	111.2±10.8	123.2±22.5	110.0±14.1	109.5±11.5	117.5±10.9
AERP	33.5±7.6	37.4±13.7	34.1±10.9	35.3±11.9	38.8±14.1
AVNERP	87.1±8.2	89.5±10.0	85.9±10.3	84.7±8.8	91.3±12.2
HPFRP	117.9±13.8	124.0±22.5	116.2±8.5	113.2±10.5	117.0±16.0
VERP	40.6±12.1	63.2±27.5*	44.7±28.1	42.6±15.5 [†]	63.1±25.9*

Data (in milliseconds) are presented as mean±SD. SA, AH, HV, and QT intervals were measured at a pacing cycle length of 200 milliseconds. In the present experimental protocol, the atrioventricular node usually became refractory to premature extrastimulation before the His-Purkinje system became refractory. Therefore, only the functional refractory period of the His-Purkinje system (HPFRP, the shortest conducted V₁V₂ interval [the interval between the last constant stimulation-evoked ventricular depolarization to the premature extrastimulation-evoked ventricular depolarization]) was measured. AB indicates aortic banding; AERP, atrial effective refractory period; AH, atrio-His bundle conduction interval; AVNERP, atrioventricular nodal effective refractory period; BCL, basic cycle length; Can, candesartan cilexetil; HV, His-ventricular conduction interval; Hyd, hydralazine; QT, ventricular repolarization time (VT interval); SA, stimulus-atrial conduction interval; Veh, vehicle; VERP, ventricular effective refractory period; and WCL, Wenckebach cycle length.

P*<0.05 and *P*<0.01 vs Sham+Veh group.

[†]*P*<0.05 vs AB+Veh group by 1-way ANOVA with a Tukey post hoc test.

control or banded rats exhibited a transmural gradient in APD or repolarization. Recordings from subendocardial layers exhibit longer APD than from subepicardial layers (Figure S4B through S4E). We observed that APDs were significantly longer in both layers from banded rats. The prolongation of APDs in both layers was proportionally prevented by candesartan cilexetil.

Candesartan Cilexetil Reduces the Incidence of Triggered Activity in LV Papillary Muscles

We determined whether LV preparations from banded rat hearts are predisposed to arrhythmic events following the addition of isoproterenol and high Ca²⁺. Figure 4A shows action potential recordings immediately after 1-minute pacing at 2, 3.3, and 5 Hz. In preparations from the sham group treated with vehicle or candesartan cilexetil, triggered action potentials seldomly occurred, whereas triggered activity was largely increased in the vehicle-treated banded group (Figure 4A and 4B). Candesartan cilexetil

administration in the banded rats significantly reduced the incidence of triggered activity at 3.3 and 5 Hz (Figure 4B).

Candesartan Cilexetil Reduces the Production of Superoxide in Myocardial Tissues

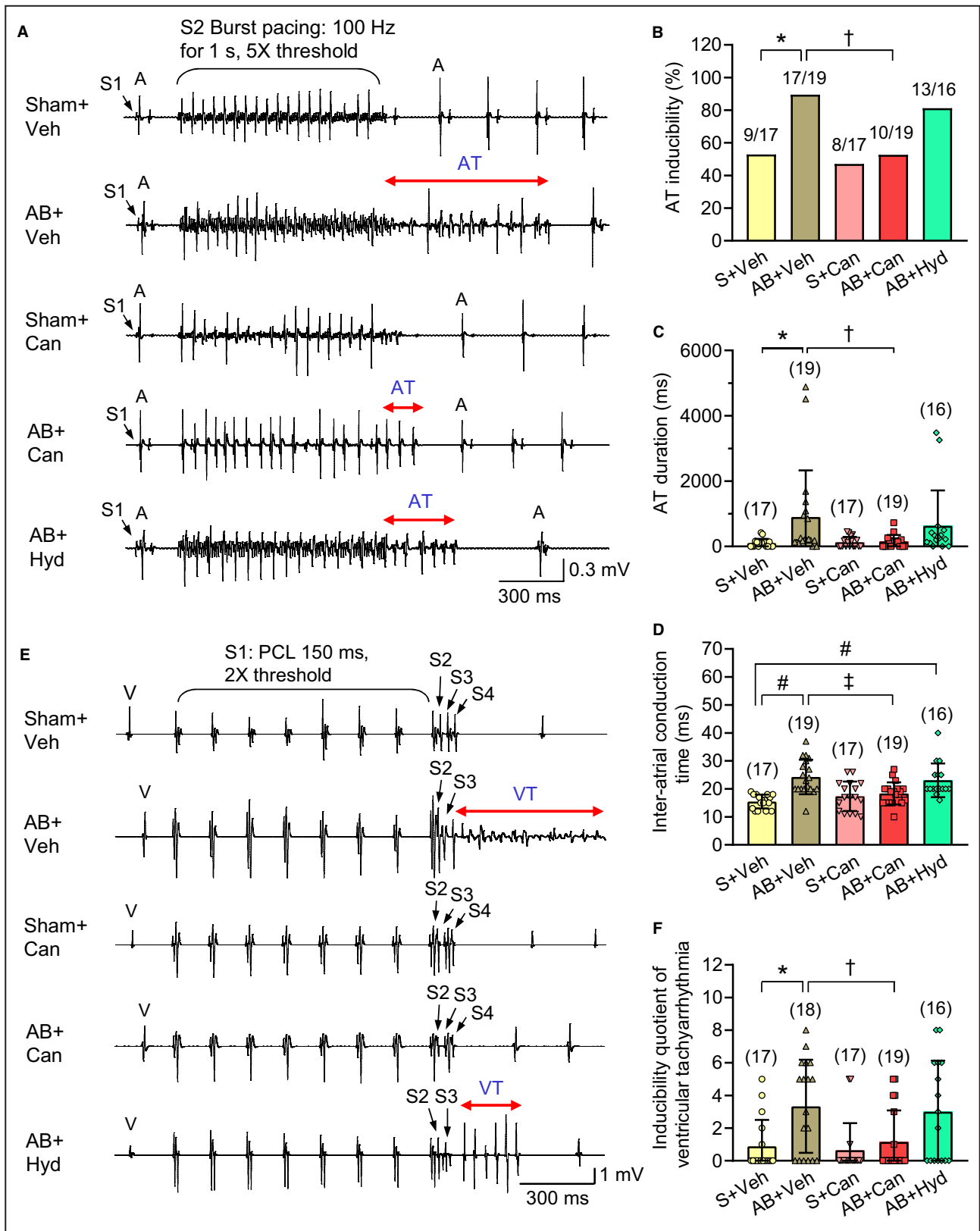
Reactive oxygen species have been shown to contribute to sustained pressure overload-induced cardiac hypertrophy, fibrosis, and pathological remodeling.²⁶ We evaluated the NADPH-dependent superoxide anion production in LV and LA tissues, and found that it was increased by AB in both tissues (Figure S5). Candesartan cilexetil treatment attenuated AB-induced superoxide production.

Candesartan Cilexetil Prevents Abnormal Myocyte Contraction and Ca²⁺ Handling

As shown in Figure 5A and 5C, both the time to peak cell shortening and the time to 50% relengthening

Figure 2. Atrial and ventricular arrhythmia vulnerabilities in Langendorff-perfused hearts.

A–D, Susceptibility to atrial tachyarrhythmias (ATs) in hearts from various groups. **A**, Representative electrograms, following 1-second burst right atrial pacing, at a basic pacing cycle length of 200 milliseconds. **B**, Percentage of hearts in each group induced to AT. Results are shown as the percentage of hearts (n) inducible into AT/total of hearts. Group comparisons for AT incidence were performed with the Fisher exact test. **C** and **D**, Mean data of AT duration (**C**) and interatrial conduction time (**D**) of the hearts from various groups, respectively. **E** and **F**, Susceptibility to ventricular tachyarrhythmias (VTs) in hearts from various groups. **E**, Examples of epicardial electrograms showing VT severity in different groups. Following 8 pacing stimuli at a basic cycle length of 150 milliseconds, extrastimuli were applied at progressively shorter coupling intervals. Polymorphic VT could be induced by 2 extrastimuli (S₁S₂=30 milliseconds and S₂S₃=60 milliseconds) in the heart from an aortic-banded rat or from a hydralazine-treated banded rat (both S₁S₂ and S₂S₃=30 milliseconds), whereas more extrastimuli (S₂–S₄) failed to induce arrhythmia in the hearts of Sham+Veh, Sham+Can, and AB+Can rats (S₁S₂, S₂S₃, and S₃S₄ all of 30 milliseconds). **F**, Inducibility quotient of VTs in hearts from various groups. The number of hearts in each group is indicated in parentheses. **C**, **D**, and **F**, Values are presented as mean±SD and were analyzed by 1-way ANOVA with a Tukey post hoc test. **P*<0.05 and [#]*P*<0.001 vs Sham+Veh group. [†]*P*<0.05 and [‡]*P*<0.01 vs AB+Veh group. AB indicates aortic banding; Can, candesartan cilexetil; Hyd, hydralazine; and Veh, vehicle.



were significantly prolonged, with no change in fractional shortening in the banded-group myocytes compared with sham controls. Similarly, both the time course of rising and that of decay of the Ca²⁺

transients were prolonged, and the amplitude of Ca²⁺ transients tended to be lower in the banded group (Figure 5A and 5B). Candesartan cilixelil treatment in banded rats corrected the abnormal

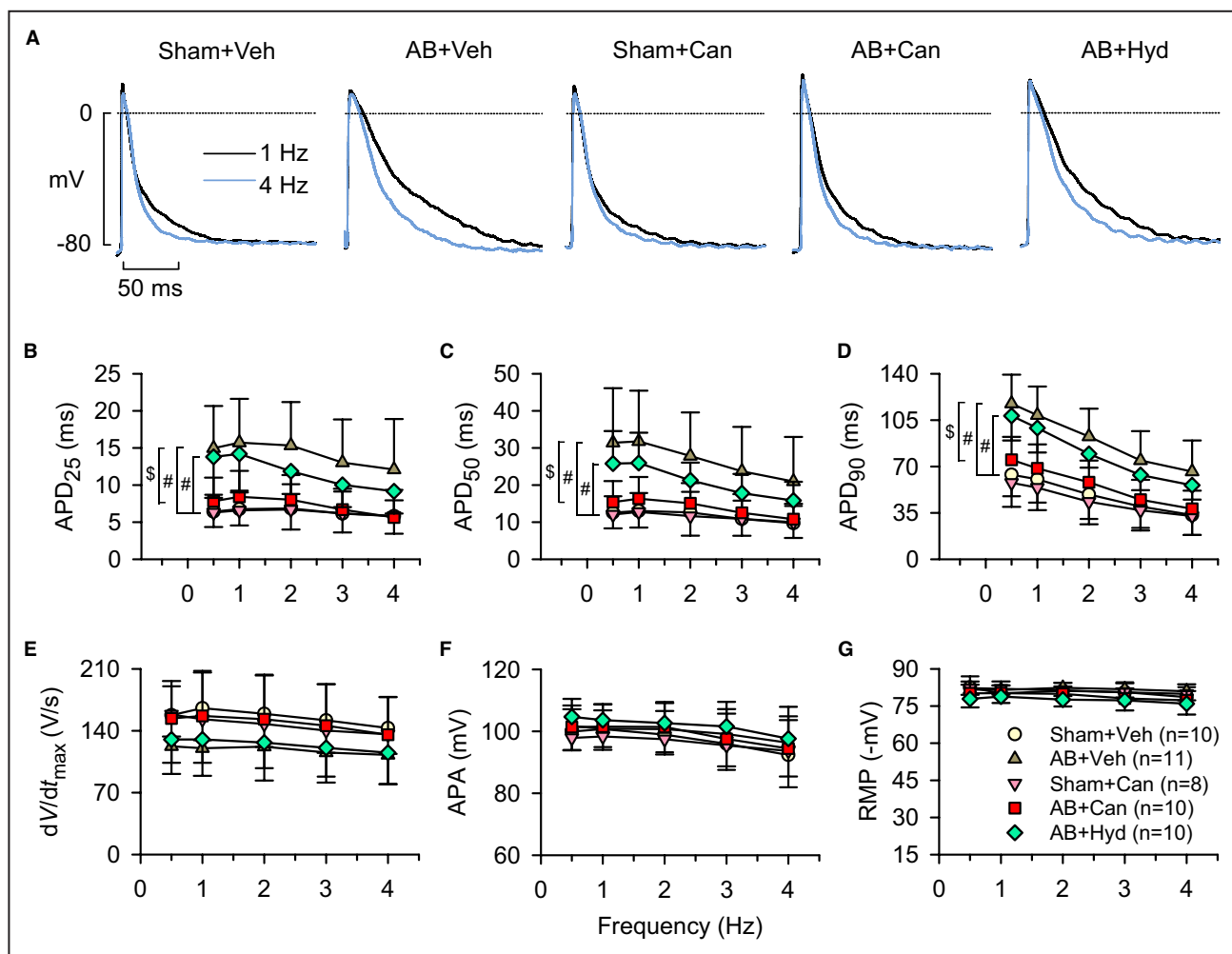


Figure 3. Transmembrane action potential variables in left ventricular papillary muscles isolated from various group hearts. **A**, Original records of superimposed action potential driven at 1 and 4 Hz. **B–G**, Frequency dependence of action potential duration (APD) at the 25%, 50%, and 90% repolarization levels (APD₂₅, APD₅₀, APD₉₀), maximal upstroke velocity (dV/dt_{max}), action potential amplitude (APA), and resting membrane potential (RMP) in all groups. Data are presented as mean \pm SD. # P <0.001 vs Sham+Veh group and \$ P <0.001 vs AB+Veh group by 2-way ANOVA with a Tukey post hoc test. The averaged slope of APD₂₅ restitution curve was -0.22 ± 0.66 , -0.86 ± 1.33 , -0.17 ± 0.37 , -0.75 ± 0.59 , and -1.52 ± 1.78 ms/Hz (P =not significant by 1-way ANOVA) in Sham+Veh, AB+Veh, Sham+Can, AB+Can, and AB+Hyd group, respectively. The corresponding value for APD₅₀ was -0.91 ± 0.74 , -3.08 ± 2.46 , -0.70 ± 0.60 , -1.53 ± 0.91 , and -3.15 ± 2.84 ms/Hz (P =not significant by 1-way ANOVA); for APD₉₀ was -9.03 ± 2.12 , -15.27 ± 6.14 (P <0.05 vs. Sham+Veh by 1-way ANOVA with a Tukey post hoc test), -7.43 ± 2.91 , -10.54 ± 2.99 , and -15.45 ± 6.46 ms/Hz (P <0.05 vs Sham+Veh by 1-way ANOVA with a Tukey post hoc test), respectively. AB indicates aortic banding; Can, candesartan cilexetil; Hyd, hydralazine; and Veh, vehicle.

kinetics of cell shortening and relengthening, normalized the amplitude and decay time constant of Ca²⁺ transients, and tended to normalize the time to peak Ca²⁺ transients.

We next assessed the rate dependency of Ca²⁺ transient and contractility. Over the frequency range of 0.5 to 2 Hz, myocytes from all groups exhibited a frequency-dependent increase in resting and peak Ca²⁺ transient, and the amplitude of the Ca²⁺ transient (Figure 6A). No differences in the normalized frequency–Ca²⁺ transient relationship were observed among the 4 groups (Figure 6A and 6B). A parallel positive contraction–frequency relation was noted in

sham control myocytes; this relationship was blunted in banded-group myocytes, which could be corrected by candesartan cilexetil treatment (Figure 6A and 6C).

The SR Ca²⁺ content was assessed by rapid application of 10 mmol/L caffeine after 10 seconds of rest following a train of 20 pulses at 1 Hz (Figure 6D). The capacity of NCX1 for Ca²⁺ removal was assessed by the rate of decay of caffeine-induced Ca²⁺ transient. We observed no significant differences in either the caffeine-induced Ca²⁺ transient amplitude or the decay time constant among the 4 groups (Figure 6D through 6F).

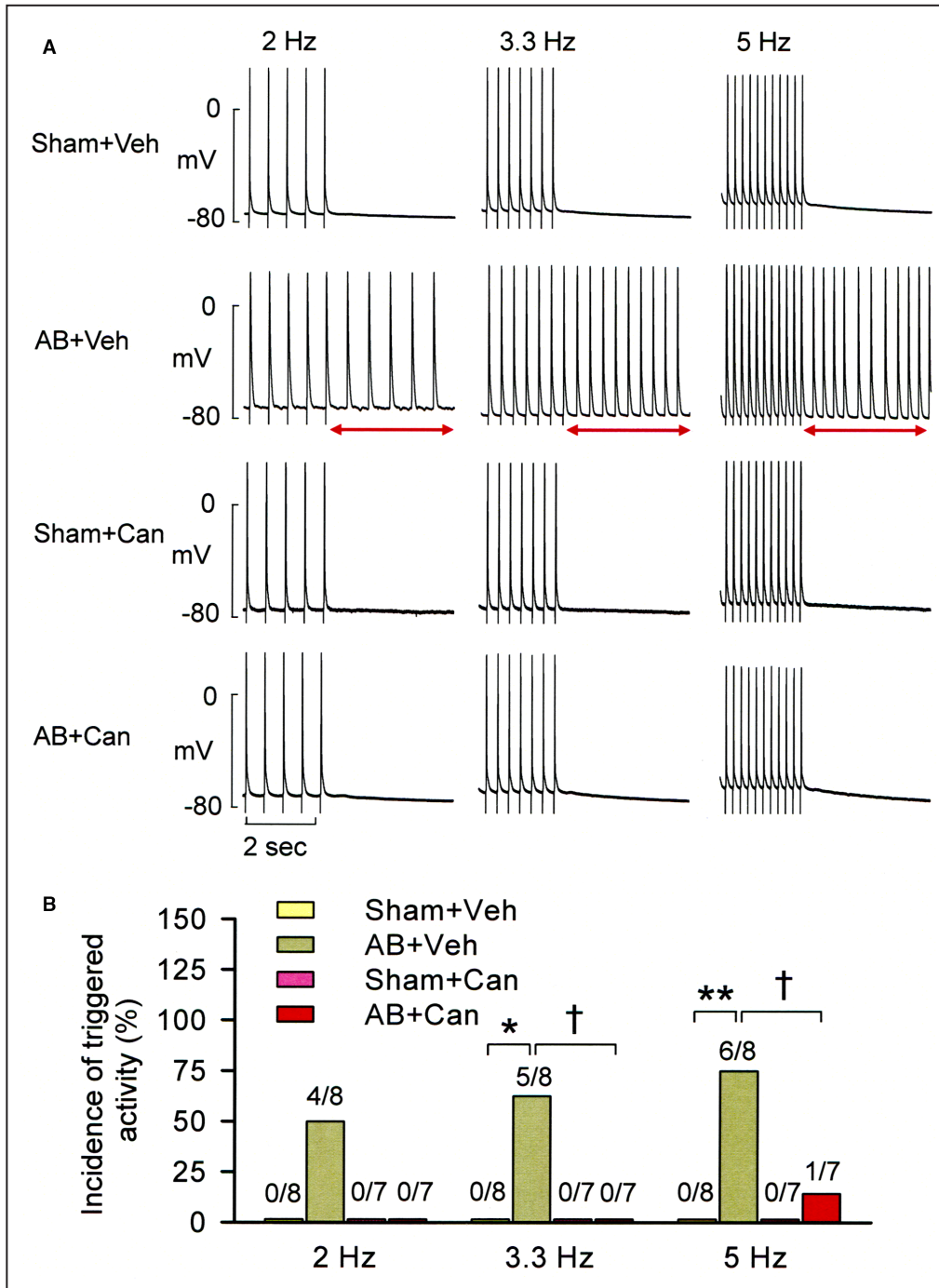


Figure 4. Triggered activity incidence in left ventricular papillary muscles isolated from various group hearts.

A, Representative tracings of action potential driven at 2, 3.3, and 5 Hz in preparations isolated from various group hearts exposed to high calcium (5.4 mmol/L) + isoproterenol (1 μM). Triggered activity (spontaneous action potentials; red double arrow line) could be induced in a preparation from AB+Veh group heart following 1-minute stimulation at all frequencies. **B**, Incidence of triggered activity in preparations isolated from various group hearts at driven frequencies of 2, 3.3, and 5 Hz. Results are shown as the percentage of preparations (n) inducible into triggered activity/total of preparations. *P<0.05 and **P<0.01 vs Sham+Veh group; †P<0.05 vs AB+Veh group by Fisher exact test. AB indicates aortic banding; Can, candesartan cilexetil; and Veh, vehicle.

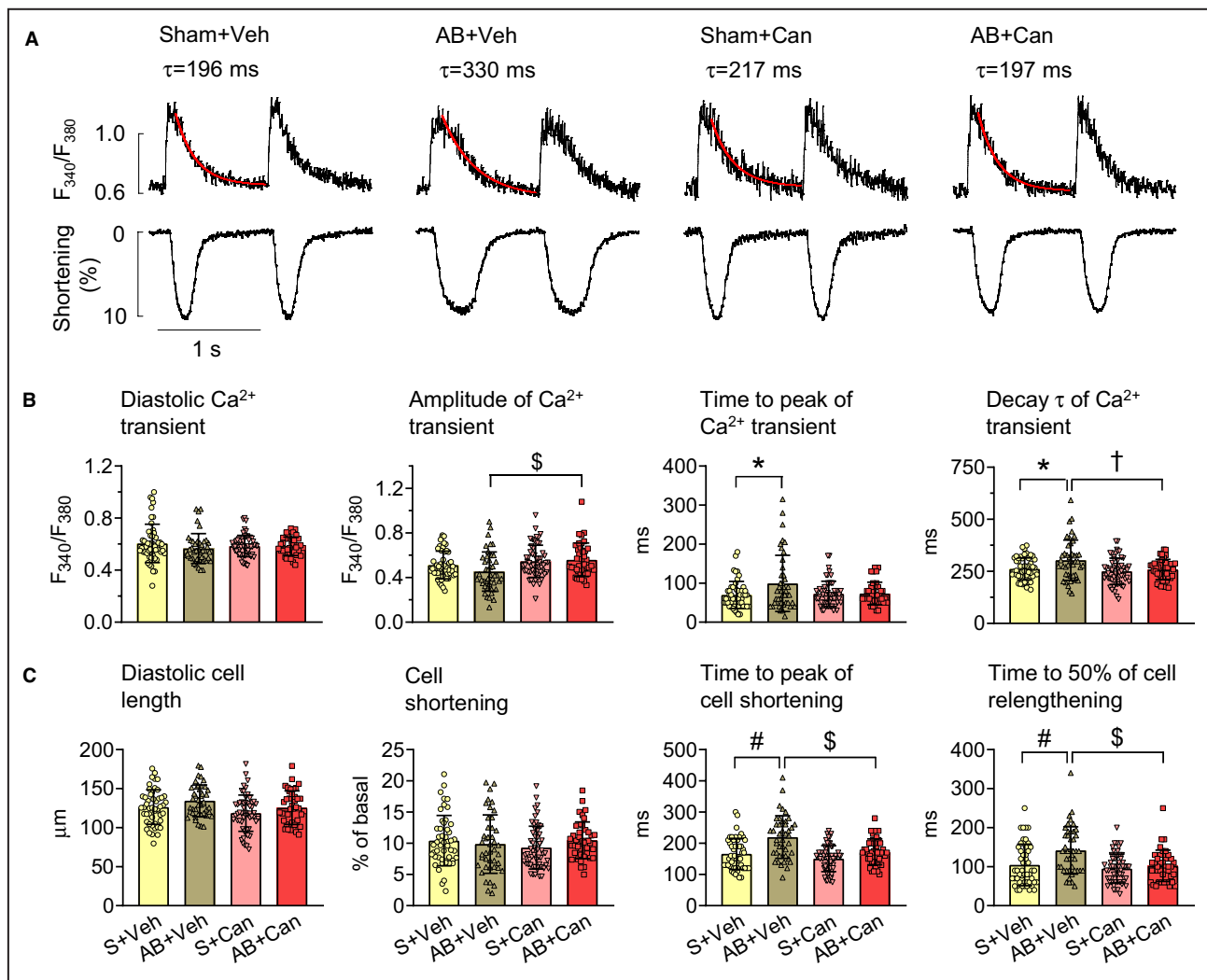


Figure 5. Effects of candesartan cilexetil treatment on cell-shortening and calcium transient kinetics in left ventricular myocytes.

A, Representative recordings of unloaded myocyte calcium (Ca^{2+}) transients (fura-2 fluorescence signal excited by 340 nm (F_{340})/fluorescence signal excited by 380 nm (F_{380})) with fitted curves (red lines) and the corresponding fraction of cell shortening at a 1-Hz pacing rate from each group. **B** and **C**, Bar graphs showing the averaged data of the parameters of Ca^{2+} transients and cell-shortening, respectively. Cell-shortening is normalized to resting cell length. Data are presented as mean \pm SD (Sham+Veh, $n=52$ cells/9 rats; AB+Veh, $n=43/8$; Sham+Can, $n=56/9$; AB+Can, $n=40/9$). * $P<0.05$ and # $P<0.001$ vs Sham+Veh; † $P<0.05$ and \$ $P<0.001$ vs AB+Veh group by linear mixed model analysis. AB indicates aortic banding; Can, candesartan cilexetil; S, sham; τ , decay time constant; and Veh, vehicle.

Candesartan Cilexetil Prevents the Abnormal Expression of Ca^{2+} -Handling Proteins

Western blotting results show that the expression level of SR SERCA2a protein was significantly decreased in the banded rat myocardium compared with the sham group, whereas the quantities of phospholamban, pSer¹⁶-phospholamban (protein kinase A (PKA) site), pThr¹⁷-phospholamban (calcium/calmodulin-dependent protein kinase II (CaMKII) site), NCX1, RyR2, pSer²⁸⁰⁸-RyR2 (PKA/CaMKII site), and pSer²⁸¹⁴-RyR2 (CaMKII site) were not different between the 2 groups (Figure 7). Candesartan cilexetil treatment in

banded rats markedly normalized the expression level of SERCA2a.

Normalization of I_{to} Density and Recovery Kinetic in LV Myocytes From Banded Rats Treated With Candesartan Cilexetil

Figure 8A presents families of representative K^{+} current tracings recorded in LV myocytes isolated from each group. The current component, remaining at the end of test pulses, was named the steady-state outward K^{+} current (I_{ss}), whereas the difference between the peak outward current and I_{ss} was taken as I_{to} . The inward current activated by hyperpolarizing pulses is mostly attributable

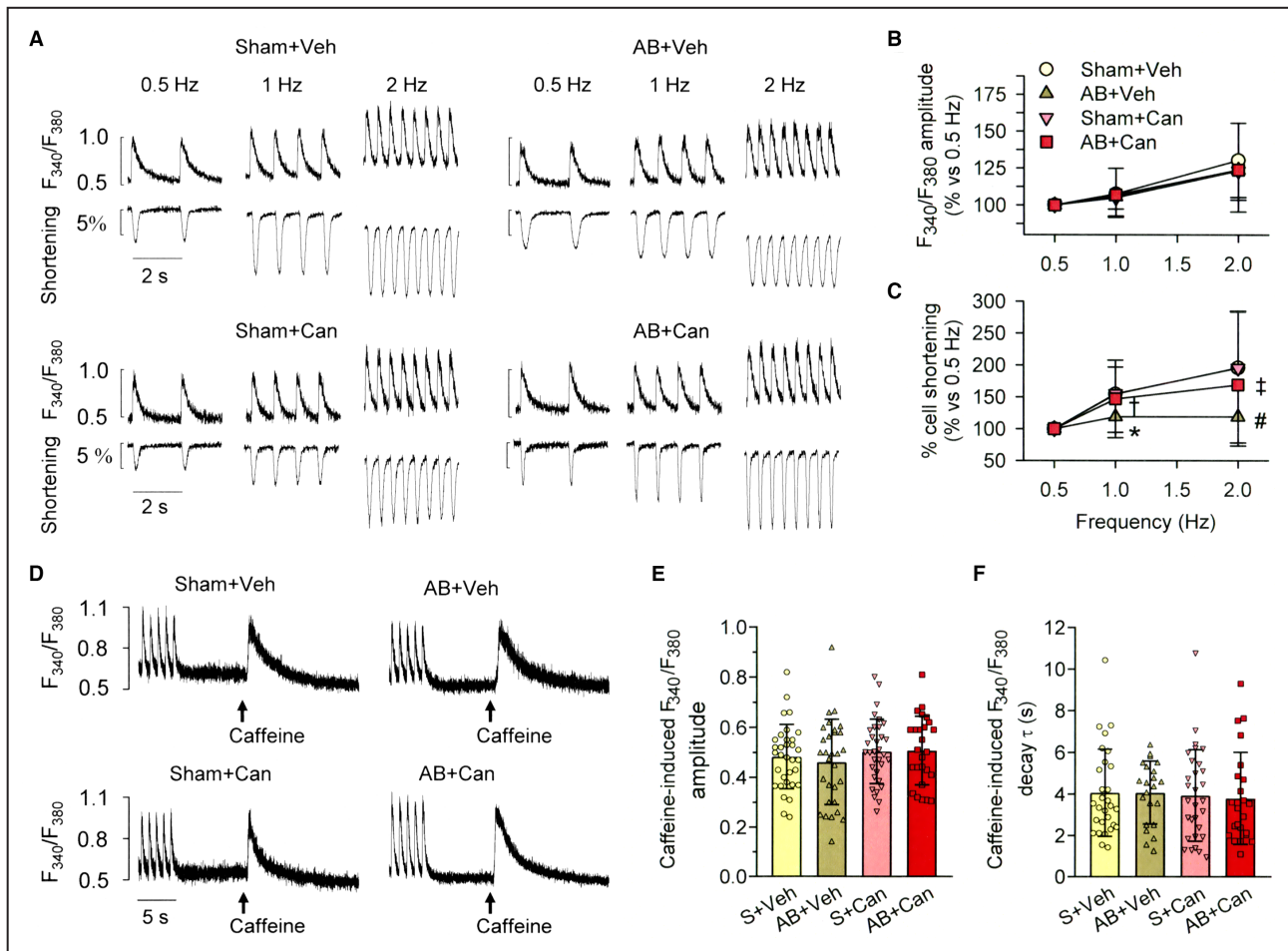


Figure 6. Rate of stimulation on contraction and calcium transients and measurement of sarcoplasmic reticulum calcium content in left ventricular myocytes.

A, Simultaneous recording of calcium (Ca^{2+}) transients (fura-2 fluorescence signal excited by 340 nm (F_{340})/fluorescence signal excited by 380 nm (F_{380})) and cell shortening at 0.5-, 1-, and 2-Hz pacing rates in each group. **B** and **C**, Relative changes in calcium transient amplitude and fraction of cell-shortening, respectively, at increasing stimulation rates. The corresponding values at 1 and 2 Hz were normalized with respect to those measured at 0.5 Hz. Data in both **(B)** and **(C)** are presented as mean \pm SD from Sham+vehicle (Veh) ($n=45$ cells/9 rats), aortic banding (AB)+Veh ($n=39/8$), Sham+candesartan cilexetil (Can) ($n=51/9$), and AB+Can ($n=37/9$) groups. * $P<0.05$ and # $P<0.001$ vs Sham+Veh; † $P<0.05$ and ‡ $P<0.01$ vs AB+Veh group by linear mixed model analysis. **D**, Representative recordings of caffeine-induced Ca^{2+} transients. Myocytes were first paced to a steady state at 1 Hz, and then pacing was stopped for 10 seconds, followed by a rapid superfusion of 10 mmol/L caffeine. **E** and **F**, Bar graphs showing the averaged data of the amplitude **(E)** and decay time constant (τ) **(F)** of the caffeine-induced Ca^{2+} transients from Sham (S)+Veh ($n=33$ cells/9 rats in **[E]**; $n=29/9$ in **[F]**), AB+Veh ($n=30/8$ in **[E]**; $n=22/6$ in **[F]**), Sham+Can ($n=33/9$ in **[E]**; $n=30/8$ in **[F]**), and AB+Can ($n=26/9$ in **[E]**; $n=23/9$ in **[F]**) groups. Data are presented as mean \pm SD.

to the inward rectifier K^+ current (I_{K1}). The mean current density–voltage (I – V) relations of peak currents (I_{to} and I_{K1}) and I_{ss} are shown in **Figure 8B** and **8C**, respectively. In banded rat myocytes, a marked reduction of I_{to} density was observed at all potentials positive to 0 mV. Treatment with candesartan cilexetil in banded rats normalized depressed I_{to} densities (**Figure 8B**). We found no significant differences between the groups in the I – V relationships of both I_{K1} and I_{ss} (**Figure 8B** and **8C**). The I_{to} decay rate was not significantly affected by either AB or candesartan cilexetil treatment (**Figure 8D**, **Table 3**).

To assess whether the observed changes in I_{to} densities resulted from altered channel gating or maximal

conductance ($G_{to, max}$), we calculated conductance–voltage (G – V) curves from the I_{to} amplitude data (**Data S1**). As summarized in **Table 3**, the estimated $G_{to, max}$ values were significantly smaller in banded-group myocytes than in sham control myocytes. Candesartan cilexetil treatment of banded rats almost completely normalized depressed $G_{to, max}$ values. The activation curves, as shown in **Figure 8E** (middle and right), were obtained from the normalized conductance ($G_{to}/G_{to, max}$) of I_{to} channels. The resultant curves were fit by the Boltzmann equation to estimate the half-activation potential (V_h) and slope (k). Candesartan cilexetil treatment had no effect on V_h or k in either sham control or

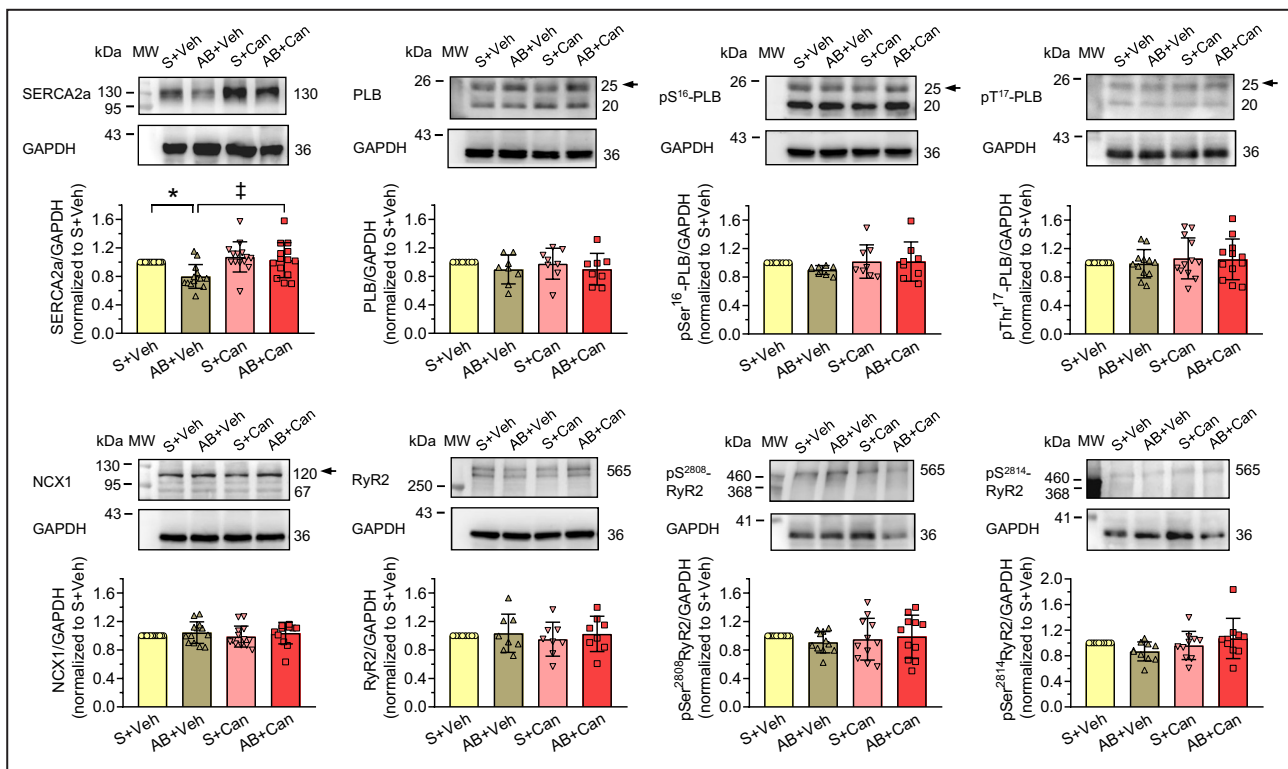


Figure 7. Western blot analysis of Ca^{2+} handling proteins' expression in left ventricular tissues from various group hearts. Top: Representative immunoblot images of calcium (Ca^{2+}) handling proteins. GAPDH was used as loading control. Numbers on the left indicate molecular mass (in kilodaltons) of marker proteins. Arrow indicates the band used for densitometric quantification. Bottom: Mean normalized densitometry of Ca^{2+} handling proteins. Bars represent the mean \pm SD of 14, 8, 8, 12, 8, 13, 11, and 10 hearts in each group for the study of SERCA2a, PLB, pSer¹⁶-PLB, pThr¹⁷-PLB, NCX1, RyR2, pSer²⁸⁰⁸-RyR2, and pSer²⁸¹⁴-RyR2, respectively. All measurements were normalized to the protein levels of GAPDH. * $P < 0.05$ vs Sham+Veh and † $P < 0.01$ vs AB+Veh group by 1-way ANOVA with a Tukey post hoc test. AB indicates aortic banding; Can, candesartan cilexetil; MW, molecular weight; NCX1, Na^{+} - Ca^{2+} exchanger 1; PLB, phospholamban; pSer¹⁶-PLB, Ser¹⁶-phosphorylated PLB; pSer²⁸⁰⁸-RyR2, Ser²⁸⁰⁸-phosphorylated RyR2; pSer²⁸¹⁴-RyR2, Ser²⁸¹⁴-phosphorylated RyR2; pThr¹⁷-PLB, Thr¹⁷-phosphorylated PLB; RyR2, ryanodine receptor Ca^{2+} release channel 2; S, sham; SERCA2a, sarco(endo)plasmic reticulum Ca^{2+} -ATPase; and Veh, vehicle.

banded rats compared with those that received vehicle treatment (Table 3). To determine whether changes in channel availability underlay the differences in peak I_{to} , we examined the voltage dependence of steady-state inactivation, and the representative current tracings from a sham-group myocyte are shown in Figure 8E (left). In Figure 8E (middle and right), the normalized magnitude of I_{to} ($I_{\text{to}}/I_{\text{to,max}}$) was plotted against conditioning potentials, and the data points were fit with the Boltzmann equation. No significant differences in steady-state voltage-dependent inactivation of I_{to} were seen among the 4 groups (Table 3).

The time dependence of I_{to} recovery from steady-state inactivation was studied using a double-pulse protocol. Figure 8F (left) illustrates the representative current tracings recorded from a sham control myocyte. The I_{to} magnitude elicited by the second pulse was expressed as a fraction of the first-pulse current and plotted against the interpulse interval (Figure 8F, middle and right). In all cases, recovery curves were best described by a monoexponential function. The

fitting data derived larger time constants in banded-group myocytes than the sham controls (Figure 8F, Table 3). Candesartan cilexetil treatment of banded rats significantly normalized the recovery time course.

L-Type Ca^{2+} Currents in LV Myocytes From Various Group Hearts

Representative L-type Ca^{2+} current ($I_{\text{Ca,L}}$) traces for each group are shown in Figure S6A. There were no significant differences in the 2 time constants of inactivation of $I_{\text{Ca,L}}$ at 0 mV, among the 4 groups of cells (Table S1). I - V relationships are shown in Figure S6B. $I_{\text{Ca,L}}$ density was not significantly different among the 4 groups. The voltage dependence of the conductance variable of $I_{\text{Ca,L}}$ activation was determined from the I - V relationships. The resultant curves were fit by the Boltzmann equation (Figure S6C). The voltage dependence of steady-state inactivation was determined with the double-pulse protocol. The relative amplitudes of $I_{\text{Ca,L}}$ were plotted against prepulse potentials and fit

to the Boltzmann distribution. There were no significant differences in steady-state voltage-dependent activation or inactivation of $I_{Ca,L}$ among the 4 group myocytes (Figure S6C and Table S1). The recovery time-course from inactivation was determined using a 2-pulse protocol. Recovery curves of $I_{Ca,L}$ in all groups of myocytes were best described by the sum of biexponentials. The fitting data gave similar time constants in all groups (Figure S6D and Table S1).

Peak Na⁺ Currents in LV Myocytes From Various Group Hearts

Whole-cell peak Na⁺ currents (I_{Na}) were elicited by a series of test potentials ranging from -70 to $+40$ mV, from a holding potential of -100 mV in 50 mmol/L extracellular Na⁺ solution. Superimposed peak I_{Na} traces were obtained from LV myocytes of various group rats (Figure S7A). Figure S7B shows the $I-V$ relationships and demonstrates that the peak I_{Na} densities in banded-rat myocytes tended to be lower than the sham controls. Similarly, there is a trend toward lower calculated maximal conductance density in banded-rat myocytes (Table S2). There were no significant differences in the time constants of inactivation of I_{Na} at -30 mV among the 4 groups of cells (Table S2). The voltage-dependent kinetics of steady-state activation and inactivation of I_{Na} were determined from the $I-V$ relationships and a double-pulse protocol, respectively (Figure S7C). The resultant curves were fit by the Boltzmann equation. There were no differences in the steady-state activation and inactivation properties among the 4 groups (Figure S7C and Table S2). Figure S7D shows the fraction of channels that recovered from inactivation. The data were best described by a monoexponential equation. The fitting results gave similar time constants in all groups (Table S2).

Candesartan Cilexetil Treatment Normalizes Expression of I_{to} Channel Proteins and mRNAs

We next analyzed the expression levels of proteins encoding various ion channels that carry $I_{Ca,L}$ ($Ca_v1.2a$), I_{Na} ($Na_v1.5$), I_{to} (Kv4.2, Kv4.3, Kv1.4, and the accessory β -subunit KChIP2), I_{SS} (Kv2.1), and I_{K1} (Kir2.1) in LV tissues from various groups. Kv4.2 and Kv4.3 proteins significantly decreased in banded-group myocardium compared with the sham controls, whereas the quantities of other proteins were not different between the 2 groups (Figure 9). Candesartan cilexetil treatment in banded rats significantly normalized the expression of both Kv4.2 and Kv4.3 proteins. We next examined the expression levels of genes encoding Kv4.2 and Kv4.3 by reverse transcription-polymerase chain reaction. In banded group LV tissues, the expression levels of both

Kv4.2 and Kv4.3 mRNAs were significantly diminished to about half of those in sham controls (Figure S8). Candesartan cilexetil treatment of banded rats significantly normalized the levels of both Kv4.2 and Kv4.3 mRNAs.

DISCUSSION

The major finding of this study is that the chronic administration of candesartan cilexetil, a potent AT₁R antagonist, immediately after AB, attenuated electromechanical, structural, and Ca²⁺ handling alterations, and subsequent vulnerability to tachyarrhythmias of the heart following pressure overload. The prevention of LV hypertrophy in banded rats by candesartan cilexetil, but not by hydralazine, in this study confirms that simply lowering arterial pressure was insufficient to prevent cardiac remodeling. It has been demonstrated that AT₁ receptors can be directly activated by mechanical stretch without involving Ang II.¹³ Further study also showed that in angiotensinogen-knockout mice lacking endogenous Ang II, candesartan, which acts as an inverse agonist, effectively inhibits pressure overload-induced cardiac hypertrophy.²⁷ Our present result shows no differences of serum or LV levels of Ang II between banded and sham control rats. We speculate that the pressure overload-induced changes in the present experimental setting should be elicited predominantly by stretch-induced AT₁R activation, which could be effectively prevented by candesartan cilexetil.

In accordance with a previous report,²⁸ we found increased LV pressure and hypertrophy measurements in rats 5 weeks after AB. We also found that systolic function was elevated, and the LV chamber was slightly dilated, indicating that the heart was in a state between moderate to severe concentric hypertrophy. The concomitant prolonged LV pressure decay τ but with unchanged end-diastolic P-V relations might be mainly attributable to the prolonged relaxation of LV myocytes. Our study suggests that chronic candesartan cilexetil treatment in banded rats prevented the accompanying cardiac hypertrophy and remodeling.

In this research, a significant increase in the APD of pressure-overloaded rat ventricles was observed, similar to previous reports.²⁸⁻³⁰ This was well-correlated with the longer corrected QT interval and ventricular effective refractory period in banded rats. All of these changes could be effectively normalized by treatment with candesartan cilexetil but not hydralazine, suggesting the electrical remodeling could be normalized by suppressing both the mechanical overload and/or the effect evoked by humoral factors (eg, Ang II) but not by lowering blood pressure alone. The LV wall showed a transmural or regional gradient in repolarization.^{31,32} Recordings from the subendocardial layer

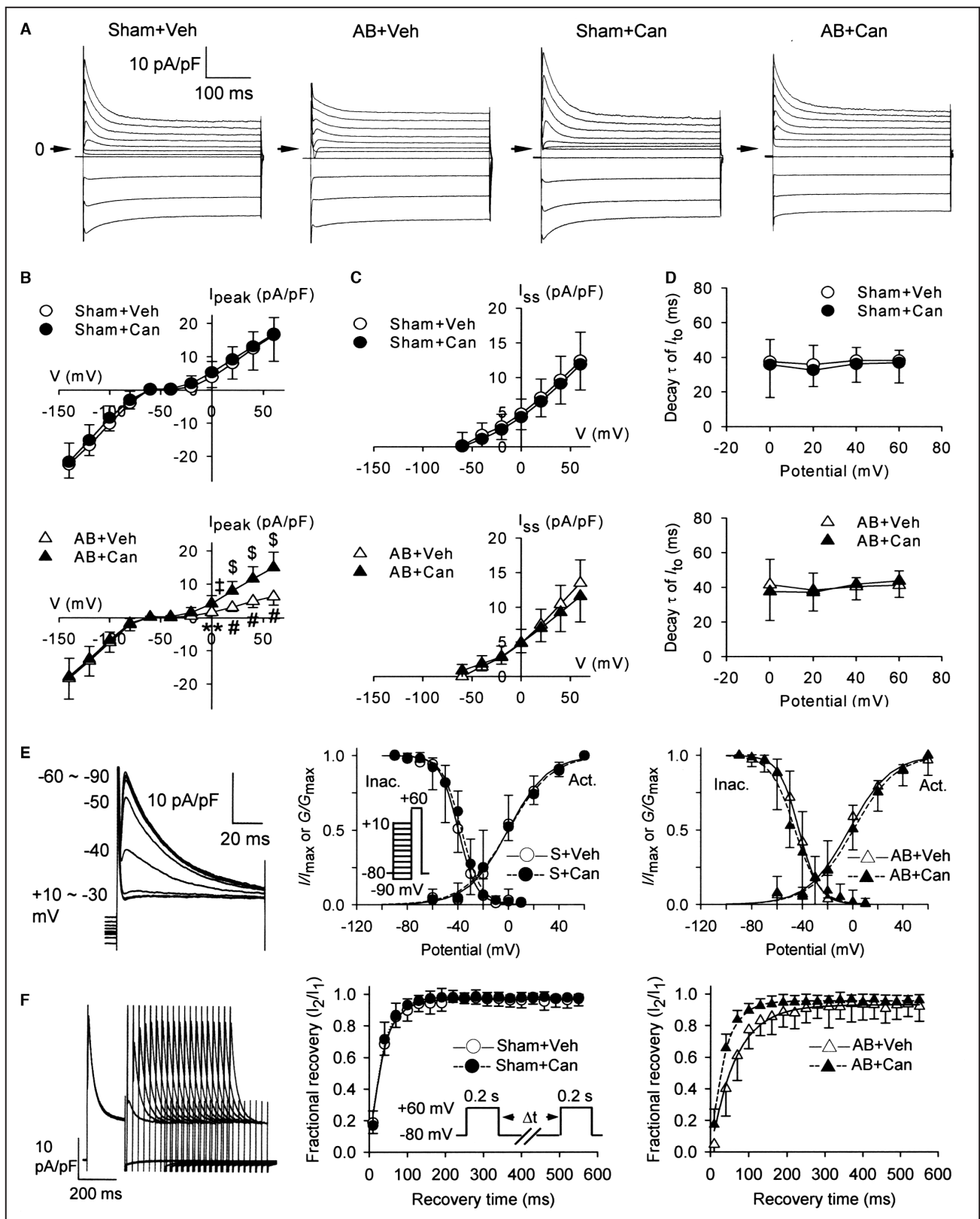


exhibit longer APD than from the subepicardial layer, with which the former expressed smaller I_{to} .³¹ A reduced regional repolarization gradient was observed

in LV myocytes from rats 7 days after AB.³² However, this phenomenon was not evident in the present observations. This discrepancy may be explained by the

Figure 8. Voltage-activated K⁺ currents in left ventricular myocytes from various group hearts.

A, Representative potassium (K⁺) current tracings recorded during depolarizing or hyperpolarizing steps from a holding potential of -80 mV to test potentials ranging between -140 and +60 mV (20-mV steps, 400-millisecond duration) in left ventricular myocytes isolated from Sham+vehicle (Veh) (Cm=229 pF), aortic banding (AB)+Veh (316 pF), Sham+candesartan cilexetil (Can) (232 pF), and AB+Can (240 pF) rats. The component remaining at the end of depolarizing pulses was named steady-state outward K⁺ current (I_{ss}), whereas the difference between the peak outward current and I_{ss} was defined as the transient outward K⁺ current (I_{to}). The arrow indicates a 0-current level. **B** and **C**, Averaged current density–voltage (I - V) relationship for I_{to} and inward rectifier K⁺ current (I_{K1}) (**B**) and I_{ss} (**C**) from LV myocytes of various groups. **D**, Voltage dependence of I_{to} inactivation rates in various groups' myocytes. The data were fit by a monoexponential function. Data in (**B**) through (**D**) are presented as mean±SD from Sham+Veh (n=14 cells/4 rats; Cm=220±46 pF), AB+Veh (n=14/5; Cm=293±55 pF), Sham+Can (n=13/5; Cm=196±56 pF), and AB+Can (n=13/5; Cm=234±95 pF) rats. ** P <0.01 and † P <0.001 vs Sham+Veh; ‡ P <0.01 and § P <0.001 vs AB+Veh group by linear mixed model analysis. **E**, Voltage-dependent steady-state activation and inactivation of I_{to} in left ventricular myocytes. Left: Representative current tracings of steady-state inactivation of I_{to} from a sham (S)-operated control myocyte. The pulse protocol is shown in the inset of middle. From a holding potential of -80 mV, cells were stepped to various conditioning potentials (between -90 and +10 mV) for 200 milliseconds before applying the 100-millisecond test pulse (to +60 mV). Middle and right: Graphs showing voltage dependence of steady-state activation (Act.) and inactivation (Inac.) for various group cells. The activation curves were obtained from the normalized conductance of I_{to} channels ($G_{to}/G_{to,max}$), which were calculated from the data of I_{to} amplitude in (**B**) and plotted as a function of the test potentials. The inactivation data are normalized to the largest peak I_{to} value obtained in each cell ($I_{to,max}$). Smooth lines drawn through the data points were the best fit to the Boltzmann equation. Activation and inactivation data are presented as mean±SD from Sham+Veh (n=14 cells/4 rats and 12 cells/4 rats, respectively), AB+Veh (n=14/5 and 14/5, respectively), Sham+Can (n=13/5 and 12/5, respectively), and AB+Can (n=13/5 and 13/5, respectively) group rats. **F**, I_{to} recovery from inactivation in left ventricular myocytes from various groups. Left: Representative tracings of recovery of I_{to} from inactivation in a sham-operated myocyte. The twin-pulse protocol (inset in middle) consisted of 2 identical 200-millisecond depolarizing pulses to +60 mV from a holding potential of -80 mV at selected intervals from 10 to 550 milliseconds. Middle and right: Fractional current recovery plotted as a function of recovery time. Data are presented as mean±SD from Sham+Veh (n=12 cells/4 rats), AB+Veh (n=14/5), Sham+Can (n=12/5), and AB+Can (n=12/5) rats. Smooth lines represent fitting of data points with a monoexponential function. Cm indicates membrane capacitance; pA, picoampere; pF, picofarad; and τ , time constant.

differences in experimental models and conditions, the degree of disease progression, and preparations from isolated myocytes or tissues.

The APD depends on a delicate balance between the depolarizing and repolarizing currents that are active during the plateau phase. Consistent with previous reports,^{29,33} our study revealed that the density and kinetics of $I_{Ca,L}$ and the expression levels of Ca_v1.2a showed no differences between the banded and sham groups, indicating that the prolonged APD may not

involve the $I_{Ca,L}$ channels. The most consistent change found in ionic currents in hypertrophied and failing animal and human hearts is reduced I_{to} density.^{8,9,30} Accordingly, we demonstrated that the I_{to} current density was downregulated in response to pressure overload, which could be prevented by candesartan cilexetil treatment. However, the I_{ss} and I_{K1} densities as well as the corresponding Kv2.1 and Kir2.1 protein levels were not changed, as reported previously,^{34,35} excluding their involvement in APD prolongation. Peak

Table 3. Kinetic Parameters of Steady-State Activation and Inactivation and Recovery of I_{to} in Ventricular Myocytes Isolated From Various Group Rats

	Sham+Veh	AB+Veh	Sham+Can	AB+Can
Activation				
n	14	14	13	13
G_{max} , pS/pF	118.6±56.9	44.9±18.0*	121.0±34.6	106.4±32.5†
V_h , mV	-0.5±7.9	-3.2±14.6	-1.8±14.9	-1.1±7.0
k , mV	14.8±1.7	14.7±4.5	14.5±3.5	16.0±3.0
Inactivation				
n	12	14	12	13
V_h , mV	-38.8±7.2	-40.7±15.1	-37.6±9.2	-40.6±12.0
k , mV	-6.0±2.4	-5.0±1.0	-5.4±1.8	-6.0±3.8
Recovery				
n	12	14	12	12
τ , ms	38.9±8.7	92.1±46.8*	36.7±9.6	43.3±9.7†

Data are presented as mean±SD. AB indicates aortic banding; Can, candesartan cilexetil; G_{max} , maximal conductance; Veh, vehicle; n, number of experiments; pS/pF, picoSiemens/picofarad; V_h and k , half-activation or inactivation voltage and slope factor, respectively; and τ , time constant for channel recovery.

* P <0.001 vs Sham+Veh group.

† P <0.001 vs AB+Veh group by linear mixed model analysis.

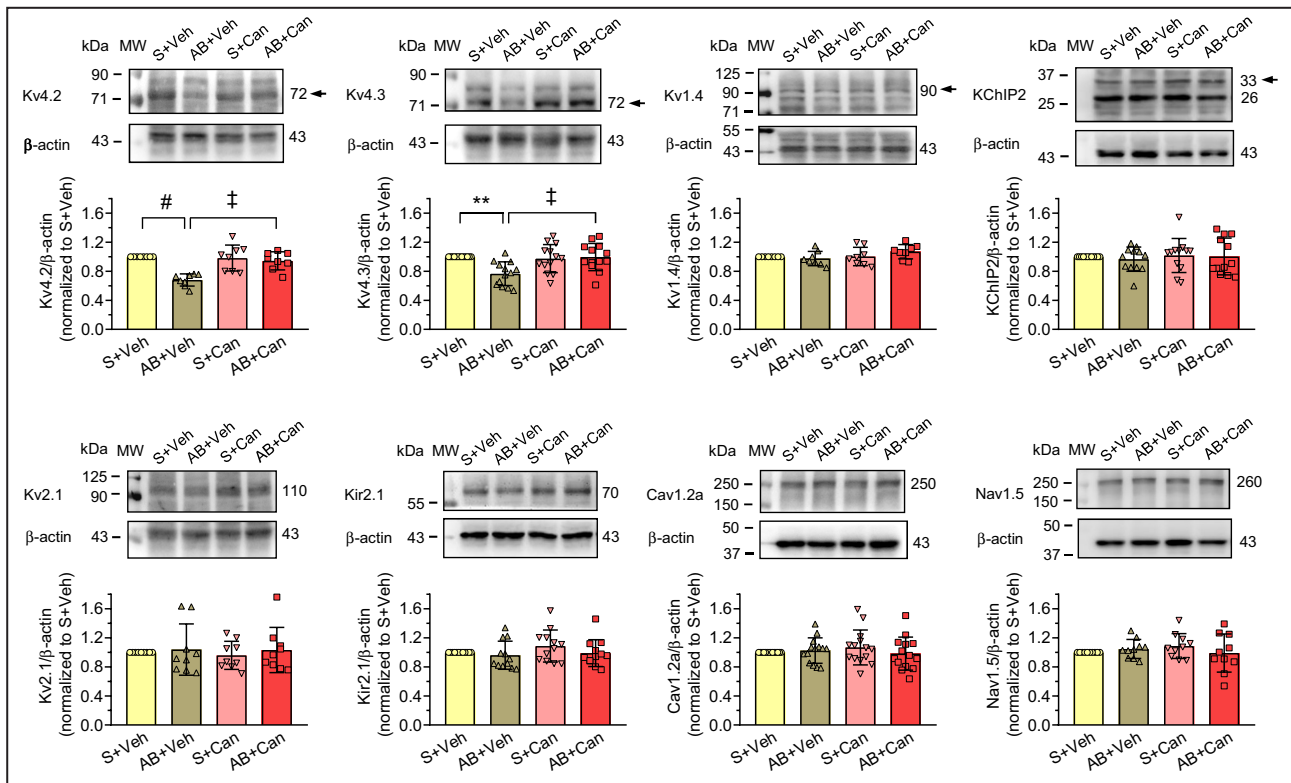


Figure 9. Western blot analysis of ion channel proteins' expression in left ventricular tissues from various group hearts.

Top in each: Representative immunoblot images of ion channel proteins. β -actin was used as the loading control. Arrow indicates the band used for densitometric quantification. Bottom in each: Mean normalized densitometry of ion channel proteins. Bars represent mean \pm SD of 8, 13, 8, 12, 9, 12, 14, and 10 hearts in each group for the study of voltage-gated potassium 4.2 channel subunit (Kv4.2), voltage-gated potassium 4.3 channel subunit (Kv4.3), voltage-gated potassium 1.4 channel subunit (Kv1.4), Kv-channel interacting protein 2 (KChIP2), voltage-gated potassium 2.1 channel subunit (Kv2.1), inwardly rectifying potassium 2.1 channel subunit (Kir2.1), voltage-gated L-type calcium 1.2a channel subunit ($\text{Ca}_v1.2a$), and voltage-gated sodium 1.5 channel subunit ($\text{Na}_v1.5$), respectively. All measurements were normalized to the protein levels of β -actin. ** $P < 0.01$ and # $P < 0.001$ vs Sham+Veh group; † $P < 0.01$ vs AB+Veh group by 1-way ANOVA with a Tukey post hoc test. AB indicates aortic banding; Can, candesartan cilexetil; S, sham; and Veh, vehicle.

I_{Na} is mainly responsible for the upstroke of cardiac action potential. Our study shows no significant changes in kinetic properties of peak I_{Na} and protein level of $\text{Na}_v1.5$, whereas the I_{Na} density tended to be less in banded rat LV preparations, which may account for the slightly lower maximal upstroke velocity of ventricular action potential and longer QRS duration in vivo in banded rats. Similar results were observed in a recent AB mice study which revealed a possible underlying mechanism of remodeling in a microtubule network and thereby impairing $\text{Na}_v1.5$ delivery in cardiomyocytes.³⁶ Chronic treatment with candesartan cilexetil prevented the decrease of maximal upstroke velocity in the banded left ventricle, perhaps mainly by preserving the peak I_{Na} density. It should be noted that the excessive LV fibrosis-mediated slow conduction may contribute to QRS prolongation in banded rats. However, we found that the prolonged QRS interval could not be completely corrected by candesartan cilexetil, albeit the fibrosis was partially prevented.

There were no changes in the steady-state activation and inactivation kinetics despite the mildly slower

recovery of I_{to} in the banded group myocytes, suggesting that reduced channel density is a likely main cause for the downregulation of I_{to} . In mammalian hearts, I_{to} has 2 components, as follows: (1) fast inactivating I_{to} ($I_{\text{to},f}$), which is encoded by Kv4.2, Kv4.3, and KChIP2,³⁷ and (2) slowly inactivating I_{to} ($I_{\text{to},s}$), which is encoded by Kv1.4. In rat LV hypertrophy, Kv4.2 and Kv4.3 mRNA are downregulated with no accompanying change in Kv1.4 mRNA.³⁴ Our results further confirmed the downregulation of both Kv4.2 and Kv4.3 protein and mRNA levels, with no changes in Kv1.4 or KChIP2 protein in the hypertrophied left ventricle. Chronic candesartan cilexetil treatment preserved the I_{to} density accompanied by normal recovery kinetics in banded rat myocytes, perhaps mainly by restoring the Kv4.2 and Kv4.3 channel expression.

The mechanisms underlying the downregulation of Kv channels associated with cardiac hypertrophy have been examined previously. Experiments with spontaneously hypertensive rats suggested that AT_1R might directly be involved in downregulating I_{to} .³⁸ It has been reported that AT_1R activation decreases Kv4.3 mRNA

and proteins by destabilizing Kv4.3 mRNA in neonatal rat cardiomyocytes.³⁹ Further study demonstrated that Ang II and mechanical stretch can increase oxidative stress by activating the AT₁R–NADPH oxidase pathway to destabilize the Kv4.3 mRNA of cardiomyocytes.⁴⁰ In this study, we found that candesartan cilexetil significantly attenuated LV superoxide production and preserved mRNA levels of both Kv4.2 and Kv4.3 in banded rats, suggesting that the prevention of Kv channel remodeling might be through its interference of the AT₁R–NADPH oxidase–oxidative stress–mRNA destabilization pathway.

Membrane depolarization during an AP activates L-type Ca²⁺ channels, whereas $I_{Ca,L}$ triggers Ca²⁺ release from the SR by activating RyR2 channels. At diastole, the increased Ca²⁺ is mainly sequestered back into the SR by SERCA2 and extruded from the cytoplasm by the sarcolemmal NCX. SERCA2 activity is regulated by its inhibitor, phospholamban; when phospholamban is phosphorylated, SERCA2 inhibition is relieved.⁴¹ Our study found that the amplitude of Ca²⁺ transient and contraction were not significantly altered, whereas their decline was markedly prolonged in banded-group myocytes, further suggesting a stage of moderate-to-severe hypertrophy was established.⁴² In line with others' findings,^{43–45} the decreased SERCA2 expression, with no changes in the total and phosphorylated phospholamban levels, may lead to a slower rate of Ca²⁺ reuptake. Restoring the impaired SR Ca²⁺ recycling and relaxation by candesartan cilexetil may be related to the preserving SERCA2 expression. As previously reported,⁴⁶ our study found no difference in RyR2 expression between the banded and sham groups. Thus, a possible explanation for the prolonged time to reach peak Ca²⁺ transient and cell-shortening with normal $I_{Ca,L}$ density and kinetics observed in banded-group myocytes is that the Ca²⁺ release of RyR2 was asynchronous despite no changes at Ser2808 and/or Ser2814 phosphorylation. Another probable mechanism may originate from the slower repolarization-associated sustaining of the Ca²⁺-induced Ca²⁺ release mechanism,^{47,48} which could be restored by candesartan cilexetil treatment. Consistent with the literature,⁴⁹ we observed no change in NCX function in banded myocytes, which was well-correlated with no change in NCX expression. Despite decreased Ca²⁺ uptake to SR, the unchanged amplitudes of Ca²⁺ transient, SR Ca²⁺ content, and contraction after AB could be explained partly by the prolonged AP and slower repolarization, which may indirectly slow $I_{Ca,L}$ decline and counteract the activity of forward-mode NCX,⁴⁷ thereby maintaining the SR Ca²⁺ content.

Myocardium from a failing heart shows a blunted contraction–frequency relationship, in contrast with that from a normal one where the contractility increases at faster frequencies,⁵⁰ possibly because of

a concomitant increase in SR Ca²⁺ content and cytosolic Ca²⁺ transients.⁴¹ We observed a similar result but without changes in the positive Ca²⁺ transients–frequency relationship among banded-rat myocytes, which could be attributable to the reduced myofilament Ca²⁺-sensitivity.⁵¹ Candesartan cilexetil maintained the normal contraction–frequency relationship possibly through preserving the myofilament Ca²⁺-sensitivity, which may improve contractility reserve and exercise tolerance in individuals with cardiac hypertrophy or failure.

The mechanisms underlying pressure overload-associated arrhythmia are multifactorial and may involve both cellular and structural remodeling.^{23,28} Cardiac fibrosis and hypertrophy, with impaired cellular coupling and impulse propagation, could contribute to the occurrence of reentrant arrhythmias. Prolonged APD might predispose a patient to early afterdepolarization, which in turn can promote triggered activity.⁶ Furthermore, action potential prolongation and a steeper APD restitution curve are known to create a substrate for reentry. Additionally, the impaired Ca²⁺ uptake by the SR can favor the oscillatory release of Ca²⁺ and the occurrence of delayed afterdepolarization-mediated triggered arrhythmias. Our work confirmed that LV tissues of banded rats were more susceptible to develop triggered activity than control tissues under conditions of adrenergic stress. By normalizing the pressure overload-associated electrical and structural remodeling, as well as Ca²⁺ handling defects, candesartan cilexetil could effectively attenuate ventricular tachyarrhythmias. In addition, the blockade of AT₁R-mediated gap junctional dysfunction⁵² in hypertrophied hearts should also be considered a possible mechanism. On the other hand, the elevated afterload has hemodynamic consequences on the left atrium, resulting in atrial remodeling and arrhythmogenesis. Atrial interstitial fibrosis and the lateralization of gap junctions may contribute to conduction abnormalities and act as a substrate for atrial tachyarrhythmias in a cardiac hypertrophy model.^{53,54} Consistent with these reports,^{53,54} we found no differences in atrial effective refractory period between banded and sham group hearts. Thus, the higher susceptibility to atrial tachyarrhythmias in banded hearts may be directly linked to the fibrosis-related slowing of atrial conduction, which could be effectively abrogated by candesartan cilexetil, as was reported previously in a canine atrial fibrillation model.⁵⁵

Some limitations should be acknowledged. Our study used a rat model that exhibits many properties similar to human pressure overloading. It has been shown that the electrophysiological property of rat heart is different from that in human. I_{to} is the major repolarization current in rat hearts, which display much shorter APD.³⁷ In human hearts, I_{to} contributes

to the early repolarization, whereas the rapid type (I_{Kr}) and slow type (I_{Ks}) delayed outward K^+ currents play a prominent role in late phase repolarizations.³⁷ Several lines of evidence suggest that the most consistently downregulated K^+ current in mammalian cardiac hypertrophy/failure is I_{to} .^{7–9} However, downregulations of other repolarizing currents contributing to prolonged APD in humans have been reported.⁸ Nevertheless, evidence suggests that the channels that mediate the early repolarization are highly conserved between humans and murine rodents.³⁷ In this context, the modulations of I_{to} remodeling as examined in our study should have important implications for cardiac hypertrophy/failure in humans. On the other hand, although candesartan cilexetil corrected most of the pressure overload-induced abnormalities, the preventions of right ventricular hypertrophy and QRS prolongation are not evident in the present setting. Further studies are needed to examine the underlying causes.

In conclusion, we demonstrated herein that candesartan cilexetil attenuated pressure overload-induced electromechanical and structural remodeling and Ca^{2+} handling dysfunction. The normalization of the electrical abnormalities seems mainly related to the preservation of I_{to} current densities. Consequently, all these beneficial effects may contribute to a lower susceptibility to arrhythmias in pressure-overloaded hearts. Our results support the idea that it is necessary to use antihypertensive drugs, with potent effects to prevent cardiac remodeling, for treating hypertensives with cardiac hypertrophy or failure.

ARTICLE INFORMATION

Received October 9, 2021; accepted March 31, 2022.

Affiliations

Graduate Institute of Clinical Medicinal Sciences, College of Medicine, Chang Gung University, Tao-Yuan, Taiwan (G.-J.C.); Cardiovascular Division of Medicine, Chang Gung Memorial Hospital, Tao-Yuan, Taiwan (G.-J.C., Y.-H.Y., W.-J.C., Y.-S.K., Y.-J.L.); Department of Respiratory Therapy, College of Medicine, Chang Gung University, Tao-Yuan, Taiwan (Y.-J.L.); Genomic Medicine Research Core Laboratory, Chang Gung Memorial Hospital, Tao-Yuan, Taiwan (Y.-S.L.); and Department of Biotechnology, Ming Chuan University, Tao-Yuan, Taiwan (Y.-S.L.).

Sources of Funding

The present work was supported by grants from the Ministry of Science and Technology of Taiwan (NSC96-2320-B-182-026-MY3) and from Chang Gung Medical Research Foundation (CMRPD160082, CMRPD170502, and BMRP468).

Disclosures

None.

Supplemental Material

Data S1
Table S1–S2
Figure S1–S8

REFERENCES

- Levy D, Garrison RJ, Savage DD, Kannel WB, Castelli WP. Prognostic implications of echocardiographically determined left ventricular mass in the Framingham Heart Study. *N Engl J Med*. 1990;322:1561–1566. doi: [10.1056/NEJM199005313222203](https://doi.org/10.1056/NEJM199005313222203)
- Kang YJ. Cardiac hypertrophy: a risk factor for QT-prolongation and cardiac sudden death. *Toxicol Pathol*. 2006;34:58–66. doi: [10.1080/01926230500419421](https://doi.org/10.1080/01926230500419421)
- Haider AW, Larson MG, Benjamin EJ, Levy D. Increased left ventricular mass and hypertrophy are associated with increased risk for sudden death. *J Am Coll Cardiol*. 1998;32:1454–1459. doi: [10.1016/S0735-1097\(98\)00407-0](https://doi.org/10.1016/S0735-1097(98)00407-0)
- Tomaselli GF, Marban E. Electrophysiological remodeling in hypertrophy and heart failure. *Cardiovasc Res*. 1999;42:270–283. doi: [10.1016/S0008-6363\(99\)00017-6](https://doi.org/10.1016/S0008-6363(99)00017-6)
- Wickenden AD, Kaprielian R, Kassiri Z, Tsoporis JN, Tsushima R, Fishman GI, Backx PH. The role of action potential prolongation and altered intracellular calcium handling in the pathogenesis of heart failure. *Cardiovasc Res*. 1998;37:312–323. doi: [10.1016/S0008-6363\(97\)00256-3](https://doi.org/10.1016/S0008-6363(97)00256-3)
- Tomaselli GF, Beuckelmann DJ, Calkins HG, Berger RD, Kessler PD, Lawrence JH, Kass D, Feldman AM, Marban E. Sudden cardiac death in heart failure. The role of abnormal repolarization. *Circulation*. 1994;90:2534–2539. doi: [10.1161/01.CIR.90.5.2534](https://doi.org/10.1161/01.CIR.90.5.2534)
- Janse MJ. Electrophysiological changes in heart failure and their relationship to arrhythmogenesis. *Cardiovasc Res*. 2004;61:208–217. doi: [10.1016/j.cardiores.2003.11.018](https://doi.org/10.1016/j.cardiores.2003.11.018)
- Beuckelmann DJ, Nabauer M, Erdmann E. Alterations of K^+ currents in isolated human ventricular myocytes from patients with terminal heart failure. *Circ Res*. 1993;73:379–385. doi: [10.1161/01.RES.73.2.379](https://doi.org/10.1161/01.RES.73.2.379)
- Kääb S, Nuss HB, Chiamvimonvat N, O'Rourke B, Pak PH, Kass DA, Marban E, Tomaselli GF. Ionic mechanism of action potential prolongation in ventricular myocytes from dogs with pacing-induced heart failure. *Circ Res*. 1996;78:262–273. doi: [10.1161/01.RES.78.2.262](https://doi.org/10.1161/01.RES.78.2.262)
- Berridge MJ, Bootman MD, Roderick HL. Calcium signalling: dynamics, homeostasis and remodelling. *Nat Rev Mol Cell Biol*. 2003;4:517–529. doi: [10.1038/nrm1155](https://doi.org/10.1038/nrm1155)
- Baker KM, Booz GW, Dostal DE. Cardiac actions of angiotensin II: role of an intracardiac renin-angiotensin system. *Annu Rev Physiol*. 1992;54:227–241. doi: [10.1146/annurev.ph.54.030192.001303](https://doi.org/10.1146/annurev.ph.54.030192.001303)
- Sadoshima J, Izumo S. The cellular and molecular response of cardiac myocytes to mechanical stress. *Annu Rev Physiol*. 1997;59:551–571. doi: [10.1146/annurev.physiol.59.1.551](https://doi.org/10.1146/annurev.physiol.59.1.551)
- Zou Y, Akazawa H, Qin Y, Sano M, Takano H, Minamino T, Makita N, Iwanaga K, Zhu W, Kudoh S, et al. Mechanical stress activates angiotensin II type 1 receptor without the involvement of angiotensin II. *Nat Cell Biol*. 2004;6:499–506. doi: [10.1038/ncb1137](https://doi.org/10.1038/ncb1137)
- Cohn JN, Tognoni G; Valsartan Heart Failure Trial Investigators. A randomized trial of the angiotensin-receptor blocker valsartan in chronic heart failure. *N Engl J Med*. 2001;345:1667–1675. doi: [10.1056/NEJMoA010713](https://doi.org/10.1056/NEJMoA010713)
- Pfeffer MA, Swedberg K, Granger CB, Held P, McMurray JJ, Michelson EL, Olofsson B, Ostergren J, Yusuf S, Pocock S, et al. Effects of candesartan on mortality and morbidity in patients with chronic heart failure: the CHARM-Overall programme. *Lancet*. 2003;362:759–766. doi: [10.1016/S0140-6736\(03\)14282-1](https://doi.org/10.1016/S0140-6736(03)14282-1)
- Joost A, Schunkert H, Radke PW. Candesartan cilexetil: an update. *Expert Opin Pharmacother*. 2011;12:1769–1780. doi: [10.1517/14656566.2011.587000](https://doi.org/10.1517/14656566.2011.587000)
- Kojima M, Shiojima I, Yamazaki T, Komuro I, Zou Z, Wang Y, Mizuno T, Ueki K, Tobe K, Kadowaki T, et al. Angiotensin II receptor antagonist TCV-116 induces regression of hypertensive left ventricular hypertrophy in vivo and inhibits the intracellular signaling pathway of stretch-mediated cardiomyocyte hypertrophy in vitro. *Circulation*. 1994;89:2204–2211. doi: [10.1161/01.CIR.89.5.2204](https://doi.org/10.1161/01.CIR.89.5.2204)
- Choisy SC, Kim SJ, Hancox JC, Jones SA, James AF. Effects of candesartan, an angiotensin II receptor type I blocker, on atrial remodeling in spontaneously hypertensive rats. *Physiol Rep*. 2015;27:3. doi: [10.14814/phy2.12274](https://doi.org/10.14814/phy2.12274)
- Obayashi M, Yano M, Kohno M, Kobayashi S, Tanigawa T, Hironaka K, Ryouke T, Matsuzaki M. Dose-dependent effect of ANG II-receptor antagonist on myocyte remodeling in rat cardiac hypertrophy. *Am J Physiol*. 1997;273:H1824–H1831. doi: [10.1152/ajpheart.1997.273.4.H1824](https://doi.org/10.1152/ajpheart.1997.273.4.H1824)

20. Yu H, Zhao G, Li H, Liu X, Wang S. Candesartan antagonizes pressure overload-evoked cardiac remodeling through Smad7 gene-dependent MMP-9 suppression. *Gene*. 2012;497:301–306. doi: [10.1016/j.gene.2012.01.081](https://doi.org/10.1016/j.gene.2012.01.081)
21. Yusuf S, Pfeffer MA, Swedberg K, Granger CB, Held P, McMurray JJ, Michelson EL, Olofsson B, Ostergren J; Investigators CHARM, et al. Effects of candesartan in patients with chronic heart failure and preserved left-ventricular ejection fraction: the CHARM-Preserved Trial. *Lancet*. 2003;362:777–781. doi: [10.1016/S0140-6736\(03\)14285-7](https://doi.org/10.1016/S0140-6736(03)14285-7)
22. Ducharme A, Swedberg K, Pfeffer MA, Cohen-Solal A, Granger CB, Maggioni AP, Michelson EL, McMurray JJV, Olsson L, Rouleau JL, et al. Prevention of atrial fibrillation in patients with symptomatic chronic heart failure by candesartan in the Candesartan in Heart failure: Assessment of Reduction in Mortality and morbidity (CHARM) program. *Am Heart J*. 2006;152:86–92. doi: [10.1016/j.ahj.2005.06.036](https://doi.org/10.1016/j.ahj.2005.06.036)
23. Zhang C, Yasuno S, Kuwahara K, Zankov DP, Kobori A, Makiyama T, Horie M. Blockade of angiotensin II type 1 receptor improves the arrhythmia morbidity in mice with left ventricular hypertrophy. *Circ J*. 2006;70:335–341. doi: [10.1253/circj.70.335](https://doi.org/10.1253/circj.70.335)
24. Chang GJ, Yeh YH, Chen WJ, Ko YS, Pang JHS, Lee HY. Inhibition of advanced glycation end products formation attenuates cardiac electrical and mechanical remodeling and vulnerability to tachyarrhythmias in diabetic rats. *J Pharmacol Exp Ther*. 2019;368:66–78. doi: [10.1124/jpet.118.252080](https://doi.org/10.1124/jpet.118.252080)
25. Chen WJ, Yeh YH, Lin KH, Chang GJ, Kuo CT. Molecular characterization of thyroid hormone-inhibited atrial L-type calcium channel expression: implication for atrial fibrillation in hyperthyroidism. *Basic Res Cardiol*. 2011;106:163–174. doi: [10.1007/s00395-010-0149-5](https://doi.org/10.1007/s00395-010-0149-5)
26. Takimoto E, Kass DA. Role of oxidative stress in cardiac hypertrophy and remodeling. *Hypertension*. 2007;49:241–248. doi: [10.1161/01.HYP.0000254415.31362.a7](https://doi.org/10.1161/01.HYP.0000254415.31362.a7)
27. Li L, Zhou N, Gong H, Wu J, Lin L, Komuro I, Ge J, Zou YZ. Comparison of angiotensin II type 1-receptor blockers to regress pressure overload-induced cardiac hypertrophy in mice. *Hypertens Res*. 2010;33:1289–1297. doi: [10.1038/hr.2010.182](https://doi.org/10.1038/hr.2010.182)
28. Jin H, Chemaly ER, Lee A, Kho C, Hadri L, Hajjar RJ, Akar FG. Mechano-electrical remodeling and arrhythmias during progression of hypertrophy. *FASEB J*. 2010;24:451–463. doi: [10.1096/fj.09.136622](https://doi.org/10.1096/fj.09.136622)
29. Scamps F, Mayoux E, Charlemagne D, Vassort G. Calcium current in single cells isolated from normal and hypertrophied rat heart. Effects of beta-adrenergic stimulation. *Circ Res*. 1990;67:199–208. doi: [10.1161/01.RES.67.1.199](https://doi.org/10.1161/01.RES.67.1.199)
30. Tomita F, Bassett AL, Myerburg RJ, Kimura S. Diminished transient outward currents in rat hypertrophied ventricular myocytes. *Circ Res*. 1994;75:296–303. doi: [10.1161/01.RES.75.2.296](https://doi.org/10.1161/01.RES.75.2.296)
31. Clark RB, Bouchard RA, Salinas-Stefanon E, Sanchez-Chapula J, Giles WR. Heterogeneity of action potential waveforms and potassium currents in rat ventricle. *Cardiovasc Res*. 1993;27:1795–1799. doi: [10.1093/cvr/27.10.1795](https://doi.org/10.1093/cvr/27.10.1795)
32. Volk T, Nguyen TH, Schultz JH, Faulhaber J, Ehmke H. Regional alterations of repolarizing K⁺ currents among the left ventricular free wall of rats with ascending aortic stenosis. *J Physiol*. 2001;530:443–455. doi: [10.1111/j.1469-7793.2001.0443k.x](https://doi.org/10.1111/j.1469-7793.2001.0443k.x)
33. Volk T, Ehmke H. Conservation of L-type Ca²⁺ current characteristics in endo- and epicardial myocytes from rat left ventricle with pressure-induced hypertrophy. *Pflügers Arch*. 2002;443:399–404. doi: [10.1007/s004240100712](https://doi.org/10.1007/s004240100712)
34. Capuano V, Ruchon Y, Antoine S, Sant MC, Renaud JF. Ventricular hypertrophy induced by mineralocorticoid treatment or aortic stenosis differentially regulates the expression of cardiac K⁺ channels in the rat. *Mol Cell Biochem*. 2002;237:1–10. doi: [10.1023/a:1016518920693](https://doi.org/10.1023/a:1016518920693)
35. Fernández-Velasco M, Ruiz-Hurtado G, Delgado C. I_{K1} and I_f in ventricular myocytes isolated from control and hypertrophied rat hearts. *Pflügers Arch*. 2006;452:146–154. doi: [10.1007/s00424-005-0024-7](https://doi.org/10.1007/s00424-005-0024-7)
36. Rivaud MR, Agullo-Pascual E, Lin X, Leo-Macias A, Zhang M, Rothenberg E, Bezzina CR, Delmar M, Remme CA. Sodium channel remodeling in subcellular microdomains of murine failing cardiomyocytes. *J Am Heart Assoc*. 2017;6:e007622. doi: [10.1161/JAHA.117.007622](https://doi.org/10.1161/JAHA.117.007622)
37. Nerbonne JM, Kass RS. Molecular physiology of cardiac repolarization. *Physiol Rev*. 2005;85:1205–1253. doi: [10.1152/physrev.00002.2005](https://doi.org/10.1152/physrev.00002.2005)
38. Cerbai E, Crucitti A, Sartiani L, De Paoli P, Pino R, Rodriguez ML, Ginsini G, Mugelli A. Long-term treatment of spontaneously hypertensive rats with losartan and electrophysiological remodeling of cardiac myocytes. *Cardiovasc Res*. 2000;45:388–396. doi: [10.1016/S0008-6363\(99\)00344-2](https://doi.org/10.1016/S0008-6363(99)00344-2)
39. Zhang TT, Takimoto K, Stewart AF, Zhu C, Levitan ES. Independent regulation of cardiac Kv4.3 potassium channel expression by angiotensin II and phenylephrine. *Circ Res*. 2001;88:476–482. doi: [10.1161/01.RES.88.5.476](https://doi.org/10.1161/01.RES.88.5.476)
40. Zhou C, Ziegler C, Birder LA, Stewart AF, Levitan ES. Angiotensin II and stretch activate NADPH oxidase to destabilize cardiac Kv4.3 channel mRNA. *Circ Res*. 2006;98:1040–1047. doi: [10.1161/01.RES.0000218989.52072.e7](https://doi.org/10.1161/01.RES.0000218989.52072.e7)
41. Bers DM. Cardiac excitation-contraction coupling. *Nature*. 2002;415:198–205. doi: [10.1038/415198a](https://doi.org/10.1038/415198a)
42. Siri FM, Krueger J, Nordin C, Ming Z, Aronson RS. Depressed intracellular calcium transients and contraction in myocytes from hypertrophied and failing guinea pig hearts. *Am J Physiol*. 1991;261:H514–H530. doi: [10.1152/ajpheart.1991.261.2.H514](https://doi.org/10.1152/ajpheart.1991.261.2.H514)
43. de la Bastie D, Levitsky D, Rappaport L, Mercadier JJ, Marotte F, Wisnewsky C, Brovkovich V, Schwartz K, Lompre AM. Function of the sarcoplasmic reticulum and expression of its Ca²⁺-ATPase gene in pressure overload-induced cardiac hypertrophy in the rat. *Circ Res*. 1990;66:554–564. doi: [10.1161/01.RES.66.2.554](https://doi.org/10.1161/01.RES.66.2.554)
44. Levitsky D, de la Bastie D, Schwartz K, Lompre AM. Ca²⁺-ATPase and function of sarcoplasmic reticulum during cardiac hypertrophy. *Am J Physiol*. 1991;261:23–26. doi: [10.1152/ajpheart.1991.261.4.23](https://doi.org/10.1152/ajpheart.1991.261.4.23)
45. Boateng SY, Naqvi RU, Koban MU, Yacoub MH, MacLeod KT, Boheler KR. Low-dose ramipril treatment improves relaxation and calcium cycling after established cardiac hypertrophy. *Am J Physiol Heart Circ Physiol*. 2001;280:H1029–H1038. doi: [10.1152/ajpheart.2001.280.3.H1029](https://doi.org/10.1152/ajpheart.2001.280.3.H1029)
46. McCall E, Ginsburg KS, Bassani RA, Shannon TR, Qi M, Samarel AM, Bers DM. Ca flux, contractility, and excitation-contraction coupling in hypertrophic rat ventricular myocytes. *Am J Physiol*. 1998;274:H1348–H1360. doi: [10.1152/ajpheart.1998.274.4.H1348](https://doi.org/10.1152/ajpheart.1998.274.4.H1348)
47. Bouchard RA, Clark RB, Giles WR. Effects of action potential duration on excitation-contraction coupling in rat ventricular myocytes. Action potential voltage-clamp Measurements. *Circ Res*. 1995;76:790–801. doi: [10.1161/01.RES.76.5.790](https://doi.org/10.1161/01.RES.76.5.790)
48. Signore S, Sorrentino A, Borghetti G, Cannata A, Meo M, Zhou YU, Kannappan R, Pasqualini F, O'Malley H, Sundman M, et al. Late Na⁺ current and protracted electrical recovery are critical determinants of the aging myopathy. *Nat Commun*. 2015;6:8803. doi: [10.1038/ncomm59803](https://doi.org/10.1038/ncomm59803)
49. Maier LS, Brandes R, Pieske B, Bers DM. Effects of left ventricular hypertrophy on force and Ca²⁺ handling in isolated rat myocardium. *Am J Physiol*. 1998;274:H1361–H1370. doi: [10.1152/ajpheart.1998.274.4.H1361](https://doi.org/10.1152/ajpheart.1998.274.4.H1361)
50. Pieske B, Maier LS, Bers DM, Hasenfuss G. Ca²⁺ handling and sarcoplasmic reticulum Ca²⁺ content in isolated failing and nonfailing human myocardium. *Circ Res*. 1999;85:38–46. doi: [10.1161/01.res.85.1.38](https://doi.org/10.1161/01.res.85.1.38)
51. Kagaya Y, Hajjar RJ, Gwathmey JK, Barry WH, Lorell BH. Long-term angiotensin-converting enzyme inhibition with fosinopril improves depressed responsiveness to Ca²⁺ in myocytes from aortic-banded rats. *Circulation*. 1996;94:2915–2922. doi: [10.1161/01.cir.94.11.2915](https://doi.org/10.1161/01.cir.94.11.2915)
52. Yasuno S, Kuwahara K, Kinoshita H, Yamada C, Nakagawa Y, Usami S, Kuwabara Y, Ueshima K, Harada M, Nishikimi T, et al. Angiotensin II type 1a receptor signalling directly contributes to the increased arrhythmogenicity in cardiac hypertrophy. *Br J Pharmacol*. 2013;170:1384–1395. doi: [10.1111/bph.12328](https://doi.org/10.1111/bph.12328)
53. Kim SJ, Choisy SC, Barman P, Zhang H, Hancox JC, Jones SA, James AF. Atrial remodeling and the substrate for atrial fibrillation in rat hearts with elevated afterload. *Circ Arrhythm Electrophysiol*. 2011;4:761–769. doi: [10.1161/CIRCEP.111.964783](https://doi.org/10.1161/CIRCEP.111.964783)
54. Naohiko T, Osamu K, Osamu W, Yasushi T, Masahide H, Tetsunori S. New therapeutic target for the non-electrophysiological signaling in atrial fibrosis and fibrillation such as inflammation. *J Arrhythm*. 2012;28:145–154. doi: [10.1016/j.joa.2012.05.001](https://doi.org/10.1016/j.joa.2012.05.001)
55. Kumagai K, Nakashima H, Urata H, Gondo N, Arakawa K, Saku K. Effects of angiotensin II type 1 receptor antagonist on electrical and structural remodeling in atrial fibrillation. *J Am Coll Cardiol*. 2003;41:2197–2204. doi: [10.1016/S0735-1097\(03\)00464-9](https://doi.org/10.1016/S0735-1097(03)00464-9)

SUPPLEMENTAL MATERIAL

Data S1.

SUPPLEMENTAL METHODS

Ventricular tachyarrhythmia (VT) vulnerability in *ex vivo* perfused hearts

After isolation, the heart was mounted on a Langendorff perfusion apparatus, and perfused with oxygenated (95% O₂ and 5% CO₂) modified Tyrode's solution containing (in mM): 117 NaCl, 4.6 KCl, 1.0 MgCl₂, 23 NaHCO₃, 0.8 NaH₂PO₄, 2 CaCl₂ and 5.5 dextrose, equilibrated at 37°C. Ventricular epicardial electrograms were recorded by a bipolar electrode, placed on the epicardial surface of the LV apex. A bipolar pacing electrode was placed on the anterior epicardial surface of the right ventricle. VT induction was then attempted by programmed electrical stimulation at a PCL of 150 ms (S₁) with one to three (S₂, S₃, and S₄) extra-stimuli delivered after eight paced beats. The stimulation intensity was twice the threshold and 5 ms in duration. Pacing protocols were interrupted if sustained ventricular tachyarrhythmia was induced. The testing endpoint was inducing non-driven VTs. A preparation was considered noninducible when ventricular pacing produced either no ventricular premature beats or only self-terminating salvos of < 6 beats. Ventricular tachyarrhythmias including ventricular tachycardia and fibrillation were considered nonsustained when it lasted ≤ 15 beats and sustained when it lasted > 15 beats. An arrhythmia scoring system was used, as previously described:²⁴ 0, noninducible preparations; 1, nonsustained tachyarrhythmias induced with three extrastimuli; 2, sustained tachyarrhythmias induced with three extrastimuli; 3, nonsustained tachyarrhythmias induced with two extrastimuli; 4, sustained tachyarrhythmias induced with two extrastimuli; 5, nonsustained tachyarrhythmias induced with one extrastimuli; 6, sustained tachyarrhythmias induced with one extrastimuli; and 7, tachyarrhythmias induced during the eight paced beats at a PCL of 150 ms. If the heart stopped before the pacing, the arrhythmia score assigned to that heart was 8. When multiple forms of arrhythmias occurred in one heart, the highest score was used.

Western blot analysis

Frozen LV tissues were homogenized in ice-cold lysis buffer. Protein concentration was measured using a Protein Assay Reagent (Bio-Rad Laboratories, Hercules, CA, USA) and adjusted for equal loading. Protein samples (30–100 µg) were separated on 4%–20% gradient gel (Mini-Protean®

Precast gels; Bio-Rad, Hercules, CA, USA; for RyR2, pSer²⁸⁰⁸-RyR2 or pSer²⁸¹⁴-RyR2), 10% (SERCA2a, Kv4.2, Kv4.3, KChIP2, Kv1.4, Kv2.1, and Kir2.1), 15% (PLB, pSer¹⁶-PLB or pThr¹⁷-PLB), or 8% (NCX1, Cav1.2a or Nav1.5) SDS-PAGE and transferred onto PVDF membranes (PerkinElmer Life Sciences, Boston, MA, USA). Membranes were blocked and then incubated overnight at 4°C with primary antibody against RyR2 (mouse monoclonal, 1:1000; MA3-916, Thermo Fisher Scientific, MA, USA), pSer²⁸⁰⁸-RyR2 (rabbit polyclonal, 1:5000; A010-30AP, Badrilla, Leeds, UK), pSer²⁸¹⁴-RyR2 (rabbit polyclonal, 1:500; A010-31AP, Badrilla), SERCA2a (rabbit polyclonal, 1:5000; A010-20, Badrilla), PLB (mouse monoclonal, 1:2000; A010-14, Badrilla), pSer¹⁶-PLB (rabbit polyclonal, 1:2000; 07-052, Millipore, Temecula, CA, USA), pThr¹⁷-PLB (rabbit polyclonal, 1:2000; A010-13, Badrilla), NCX1 (rabbit polyclonal, 1:500; sc-30306; Santa Cruz Biotech, USA), Cav1.2a (rabbit polyclonal, 1:400; AB5156-50UL, Millipore), Nav1.5 (rabbit polyclonal, 1:500; ASC-005, Alomone labs, Jerusalem, Israel), Kv4.2 (rabbit polyclonal, 1:200; AB5360-200UL, Millipore), Kv4.3 (rabbit polyclonal, 1:200; APC-017, Alomone labs), Kv1.4 (rabbit polyclonal, 1:200; APC-007, Alomone labs), KChIP2 (rabbit polyclonal, 1:500; PA1-927, Thermo Fisher Scientific), Kv2.1 (rabbit polyclonal, 1:500; APC-012, Alomone labs), and Kir2.1 (rabbit polyclonal, 1:600; APC-026, Alomone labs). The blot was also probed by a GAPDH antibody (mouse monoclonal, 1:1000; sc-32233, Santa Cruz) or a β -actin antibody (rabbit polyclonal, 1:1000; ab8227, Abcam Inc., MA, USA) as an internal control. The membranes were then incubated with horseradish peroxidase-tagged anti-mouse IgG (1:5000, AP-124P, Millipore) or anti-rabbit IgG (1:10000, 111-035-003, Jackson ImmunoResearch Lab, Inc.) for 1 h at room temperature. The antibody-antigen complexes in all membranes were detected by the enhanced chemiluminescence detection kit (PerkinElmer) according to the manufacturer's instructions and digitized in a BioSpectrum 500 Imaging System (UVP, Upland, CA, USA). The densities of the immunoreactive bands were quantified using VisionWorks LS image software (version 6.6a; UVP).

Whole-cell patch-clamp recording

Pulse protocol and analysis

K^+ currents were elicited with depolarizing or hyperpolarizing steps from a holding potential of -80 mV to test potentials ranging between -140 and $+60$ mV (20-mV steps, 400-ms duration) with a stimulation frequency of 0.2 Hz. Voltages more positive than -30 mV activated a peak outward K^+ current and subsequently inactivated to a sustained level (I_{SS}) at the end of the pulse. A rapidly activating and inactivating I_{to} was identified as the difference between the peak and the steady-state current (I_{SS}). Voltages negative to -60 mV activated an inward current that represented the inward rectifier K^+ current (I_{K1}). To obtain the steady-state inactivation curves of I_{to} , a double-pulse protocol was used. The membrane was voltage-clamped to different conditioning potentials (from -90 to $+10$ mV) for 200 ms and then stepped to $+60$ mV for 100 ms, at which time I_{to} was fully activated. The holding potential was -80 mV, and the interval between test pulses was 5 s. The relative peak amplitudes of I_{to} ($I_{to}/I_{to, max}$) were plotted against prepulse potentials, and fitted to Boltzmann function and the voltage for half-inactivation (V_h) and slope factor (k) were calculated. To obtain the recovery curves of I_{to} from inactivation, a paired-pulse protocol was used consisting of two identical 200-ms depolarizing pulses to $+60$ mV from a holding potential of -80 mV. The prepulse–test pulse interval was varied between 10 and 550 ms. Each paired-pulse sequence was separated by a 10-s interval to allow for complete recovery of I_{to} from inactivation. The normalized recovery fraction of I_{to} ($I_{test\ pulse}/I_{prepulse}$) was plotted against the recovery times and fitted to a monoexponential function.

L-type Ca^{2+} currents ($I_{Ca,L}$) were evoked by applying the depolarizing steps to test potentials ranging between -40 and $+60$ mV (10-mV steps, 250-ms duration) from a holding potential of -80 mV, after a 150-ms prepulse to -40 mV to inactivate I_{Na} and T-type Ca^{2+} current. Steady-state inactivation of $I_{Ca,L}$ was examined with a double-pulse protocol: 1-s conditioning pulses were applied in 10-mV steps between -70 to $+20$ mV from a holding potential of -80 mV, and then the test pulse of 200-ms duration was applied to 0 mV after a 30-ms interpulse to -40 mV. The relative peak amplitudes of $I_{Ca,L}$ were plotted against prepulse potentials and fitted to Boltzmann distribution. To obtain the recovery curves of $I_{Ca,L}$ from inactivation, a paired-pulse protocol was used consisting of

two identical 250-ms depolarizing pulses to 0 mV from a holding potential of -40 mV. The prepulse–test pulse interval was varied between 40 and 4050 ms. Each paired-pulse sequence was separated by a 10-s interval to allow for complete recovery of $I_{Ca,L}$ from inactivation. The normalized recovery fraction of $I_{Ca,L}$ ($I_{\text{test pulse}}/I_{\text{prepulse}}$) was plotted against the recovery times and fitted to a bi-exponential function.

Na^+ inward currents (I_{Na}) were evoked by applying the depolarizing steps to test potentials ranging between -70 and $+40$ mV (10-mV steps, 30-ms duration) from a holding potential of -100 mV. Steady-state inactivation of I_{Na} was examined with a double-pulse protocol: 1-s conditioning pulses were applied in 10-mV steps between -140 to -40 mV from a holding potential of -80 mV, and then the test pulse of 50-ms duration was applied to -20 mV. To obtain the recovery curves of I_{Na} from inactivation, a paired-pulse protocol was used. A 50-ms prepulse was first applied from a holding potential of -100 mV to -20 mV, which was followed by a 20 ms test pulse after variable interpulse intervals ranging from 10 to 580 ms. The normalized recovery curve was fitted to a monoexponential function.

Steady-state inactivation data of voltage-activated ion channels were fitted with a Boltzmann function of the form:

$$I/I_{\text{max}} = 1/\{1+\exp[(V_m-V_h)/k]\}$$

where I gives the current amplitude and I_{max} its maximum, V_m the potential of prepulse, V_h the half-maximal inactivation potential, and k the slope factor. Conductance of voltage-activated ion channel (G) was calculated according to the equation as follows:

$$G = I/(V_m - V_{\text{rev}})$$

where I is the peak ionic current, V_{rev} is the reversal potential of this current (approximately -80 mV for I_{to} , $+70$ mV for $I_{Ca,L}$, and $+40$ mV for I_{Na}), and V_m is the test potential. The normalized G (G/G_{max}) was plotted as a function of V_m (activation curve) and analyzed by using the Boltzmann equation as follows:

$$G/G_{\text{max}} = 1/\{1+\exp[(V_h-V_m)/k]\}$$

where G_{\max} is the maximal ionic conductance, and V_h and k represent the half-maximal activation potential and a slope factor, respectively.

Table S1. Kinetic parameters of current decay, steady-state activation and inactivation, and recovery of $I_{Ca,L}$ in ventricular myocytes isolated from various group rats

	Sham+Veh	AB+Veh	Sham+Can	AB+Can
Decay				
n	10	11	10	10
τ_1 (ms)	12.8 ± 5.5	19.0 ± 7.3	15.4 ± 5.1	14.3 ± 7.9
τ_2 (ms)	66.0 ± 17.8	95.5 ± 57.8	64.8 ± 16.1	88.8 ± 30.2
Activation				
n	10	11	10	10
G_{max} (pS/pF)	130.0 ± 39.5	125.3 ± 39.7	131.0 ± 30.8	138.5 ± 27.5
V_h (mV)	-17.4 ± 4.4	-19.0 ± 4.3	-18.2 ± 1.9	-20.3 ± 4.0
k (mV)	5.0 ± 1.0	4.5 ± 0.9	4.7 ± 1.0	4.0 ± 1.2
Inactivation				
n	9	10	9	10
V_h (mV)	-34.0 ± 4.7	-31.1 ± 7.2	-33.2 ± 5.1	-28.9 ± 3.8
k (mV)	-5.8 ± 1.3	-5.8 ± 0.7	-5.8 ± 0.8	-6.0 ± 0.9
Recovery				
n	9	9	8	11
A_f	0.56 ± 0.15	0.69 ± 0.16	0.61 ± 0.20	0.70 ± 0.26
τ_f (s)	0.20 ± 0.13	0.20 ± 0.09	0.19 ± 0.10	0.21 ± 0.08
τ_s (s)	1.12 ± 0.76	1.66 ± 1.22	1.78 ± 1.50	1.23 ± 0.39

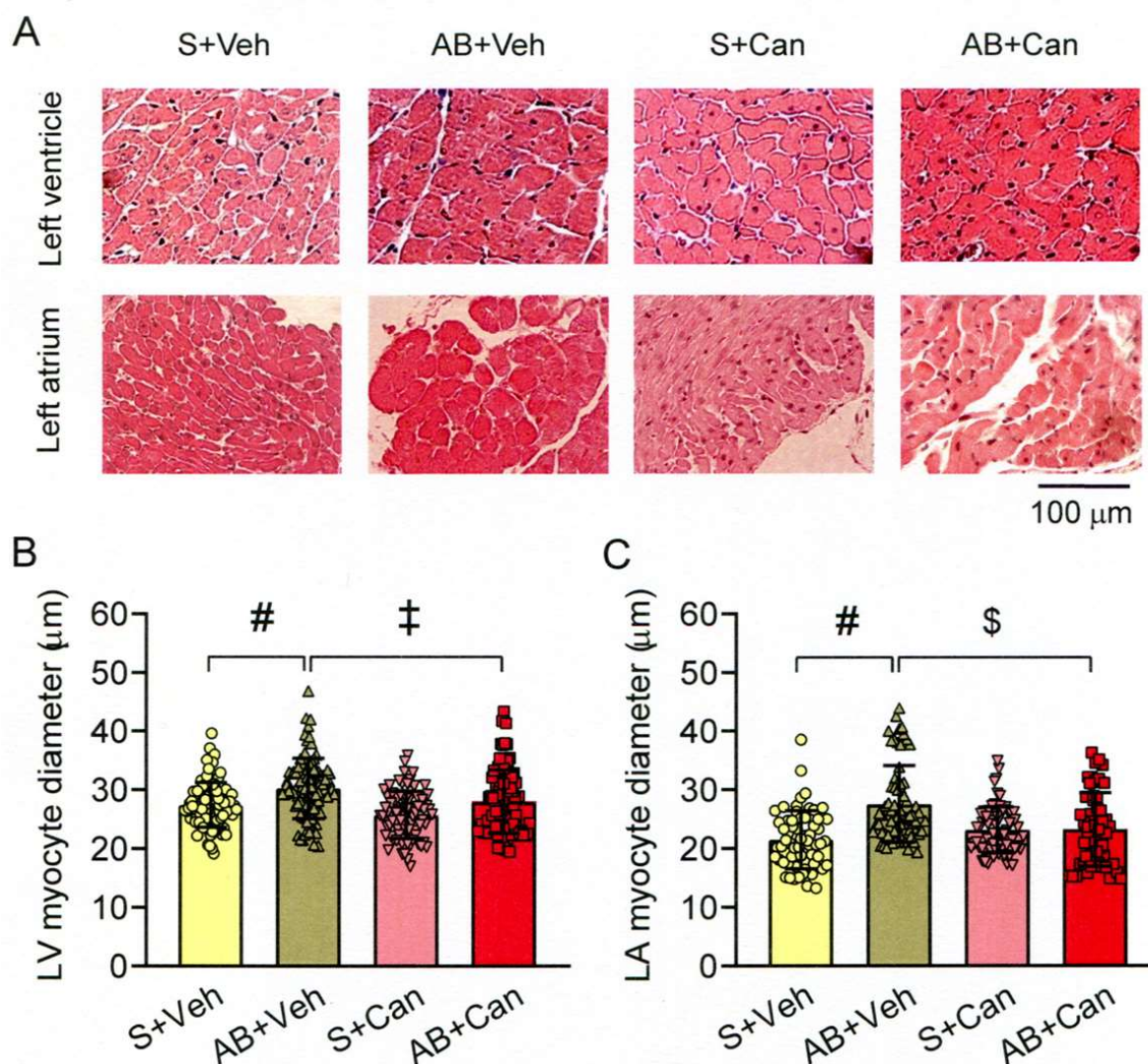
Data are presented as means \pm SD. n is number of experiments. Veh indicates vehicle; AB, aortic banding; Can, candesartan cilexetil; G_{max} , maximal conductance; τ_1 and τ_2 , fast and slow time constant for channel inactivation at 0 mV, respectively; V_h and k , half-activation or inactivation voltage and slope factor, respectively; A_f , the fast fraction of channel recovery; τ_f and τ_s , fast and slow time constant for channel recovery, respectively. Data were analyzed by linear mixed model analysis.

Table S2. Kinetic parameters of current decay, steady-state activation and inactivation, and recovery of peak I_{Na} in ventricular myocytes isolated from various group rats

	Sham+Veh	AB+Veh	Sham+Can	AB+Can
Decay				
n	14	16	12	12
τ_1 (ms)	1.66 ± 0.84	1.62 ± 0.89	1.87 ± 0.80	1.46 ± 0.85
τ_2 (ms)	5.60 ± 5.51	5.17 ± 2.87	5.87 ± 4.00	4.34 ± 4.03
Activation				
n	14	16	12	12
G_{max} (pS/pF)	296.7 ± 111.5	262.3 ± 96.8	344.7 ± 193.6	317.4 ± 119.5
V_h (mV)	-43.2 ± 7.3	-45.4 ± 11.3	-41.6 ± 7.9	-45.8 ± 7.9
k (mV)	3.0 ± 2.0	2.2 ± 0.8	3.6 ± 2.4	2.1 ± 1.0
Inactivation				
n	14	16	12	12
V_h (mV)	-81.8 ± 12.0	-84.8 ± 10.3	-81.2 ± 11.4	-79.6 ± 9.1
k (mV)	-6.8 ± 1.3	-6.5 ± 1.0	-6.8 ± 1.6	-6.2 ± 0.7
Recovery				
n	12	14	11	11
τ (ms)	22.0 ± 18.4	32.7 ± 15.9	24.6 ± 10.9	27.4 ± 19.6

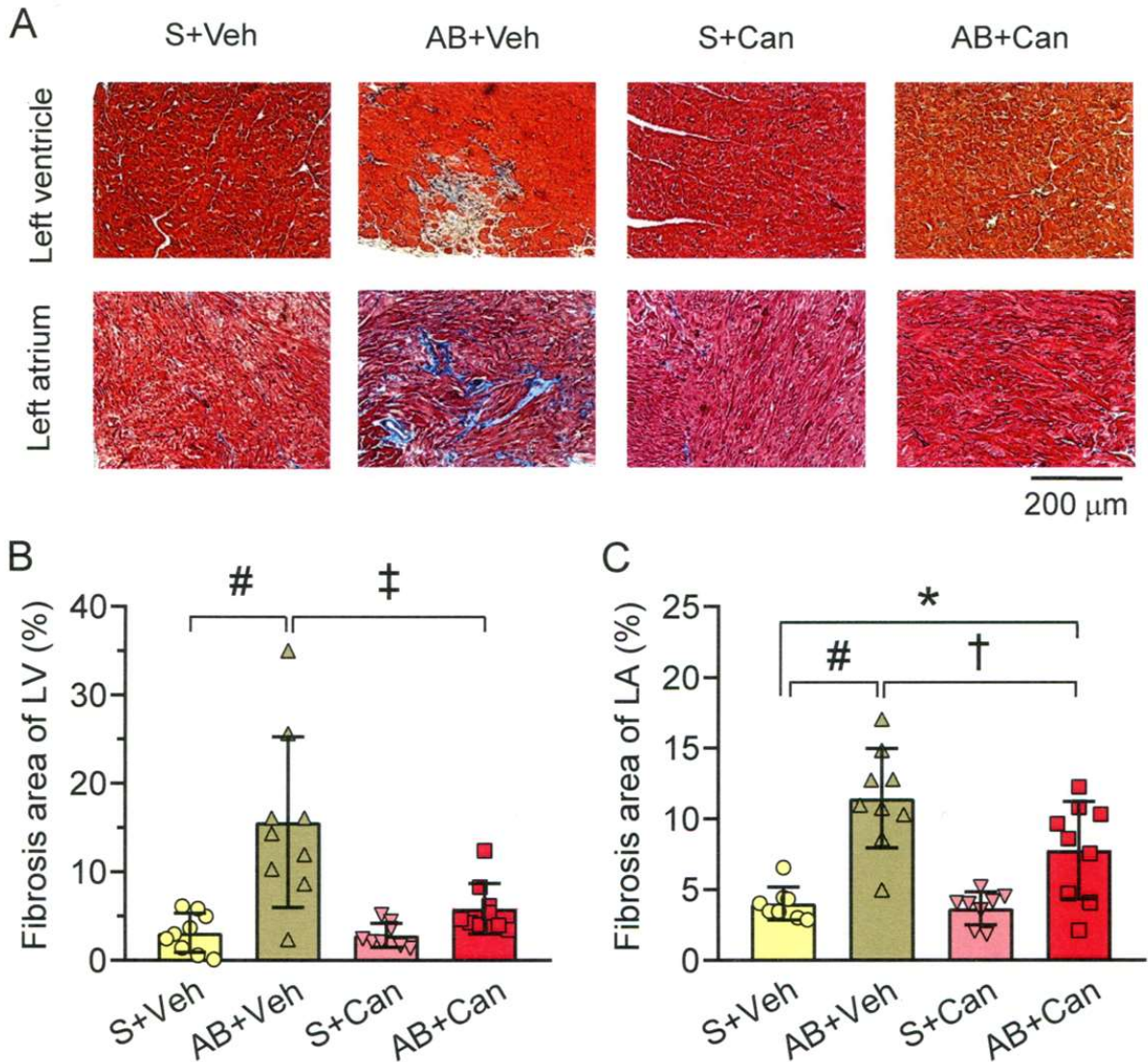
Data are presented as means \pm SD. n is number of experiments. Veh indicates vehicle; AB, aortic banding; Can, candesartan cilexetil; G_{max} , maximal conductance; τ_1 and τ_2 , fast and slow time constant for channel inactivation at -30 mV, respectively; V_h and k , half-activation or inactivation voltage and slope factor, respectively; τ , time constant for channel recovery. Data were analyzed by linear mixed model analysis.

Figure S1. Histological analyses for the hearts from various groups.



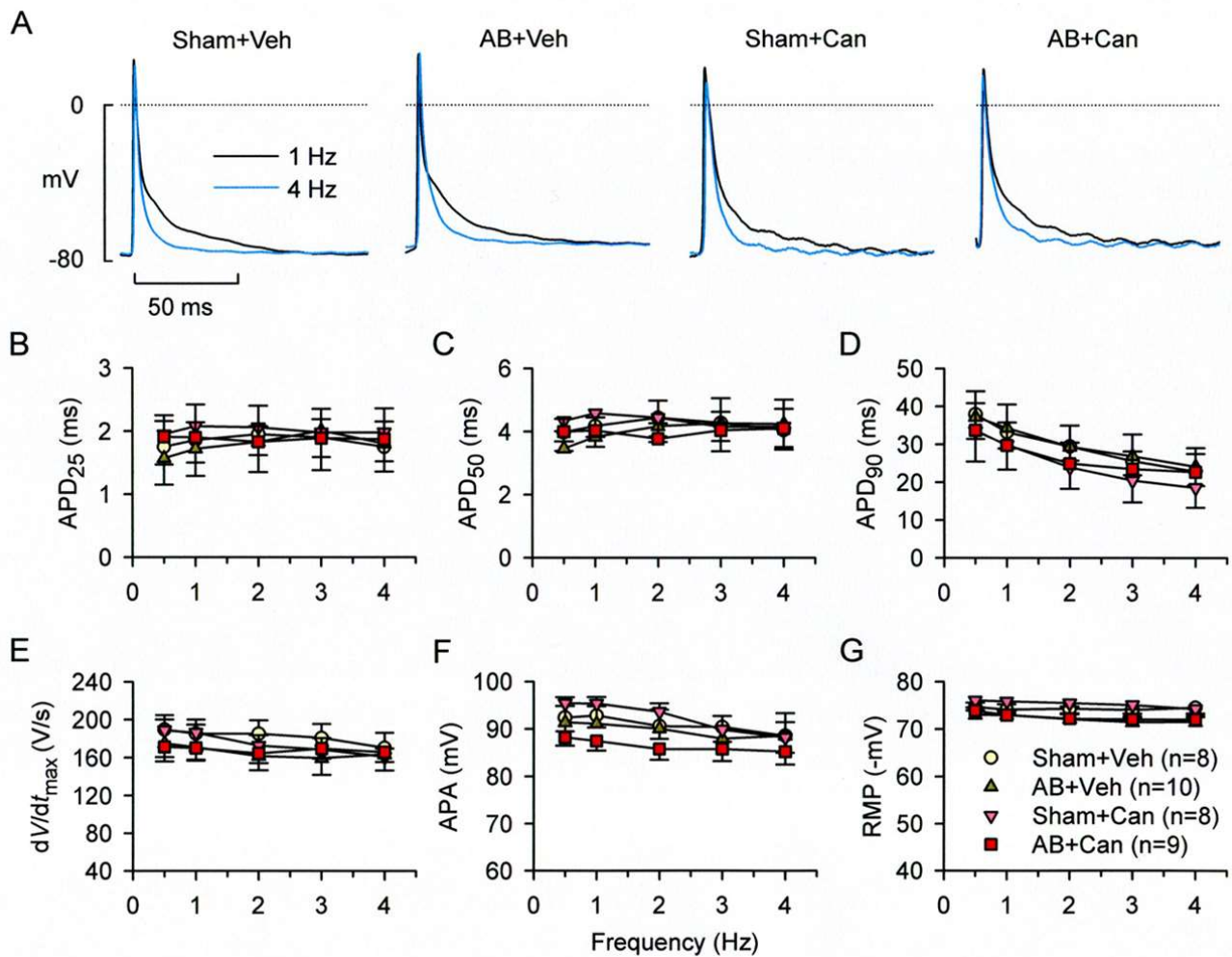
A, Representative photomicrographs of hematoxylin and eosin-stained cross-sectional sections of LV (upper panel) and left atrial (lower panel) free walls from rats of each group. **B**, Mean cardiomyocyte diameter of LV free walls calculated from sections of Sham (S)+vehicle (Veh) (n=90 myocytes/9 rats), aortic banding (AB)+Veh (n=90/9), S+candesartan cilexetil (Can) (n=80/8), and AB+Can (n=90/9) group rats. **C**, Mean cardiomyocyte diameter of left atrial free walls calculated from sections of Sham+Veh (n=60 myocytes/6 rats), AB+Veh (n=68/6), Sham+Can (n=67/7), and AB+Can (n=55/6) group rats. Data are presented as means±SD. # $P < 0.001$ vs. Sham+Veh group; ‡ $P < 0.01$ and \$ $P < 0.001$ vs. AB+Veh group by linear mixed model analysis.

Figure S2. Cardiac fibrosis analyses for the hearts from various groups.



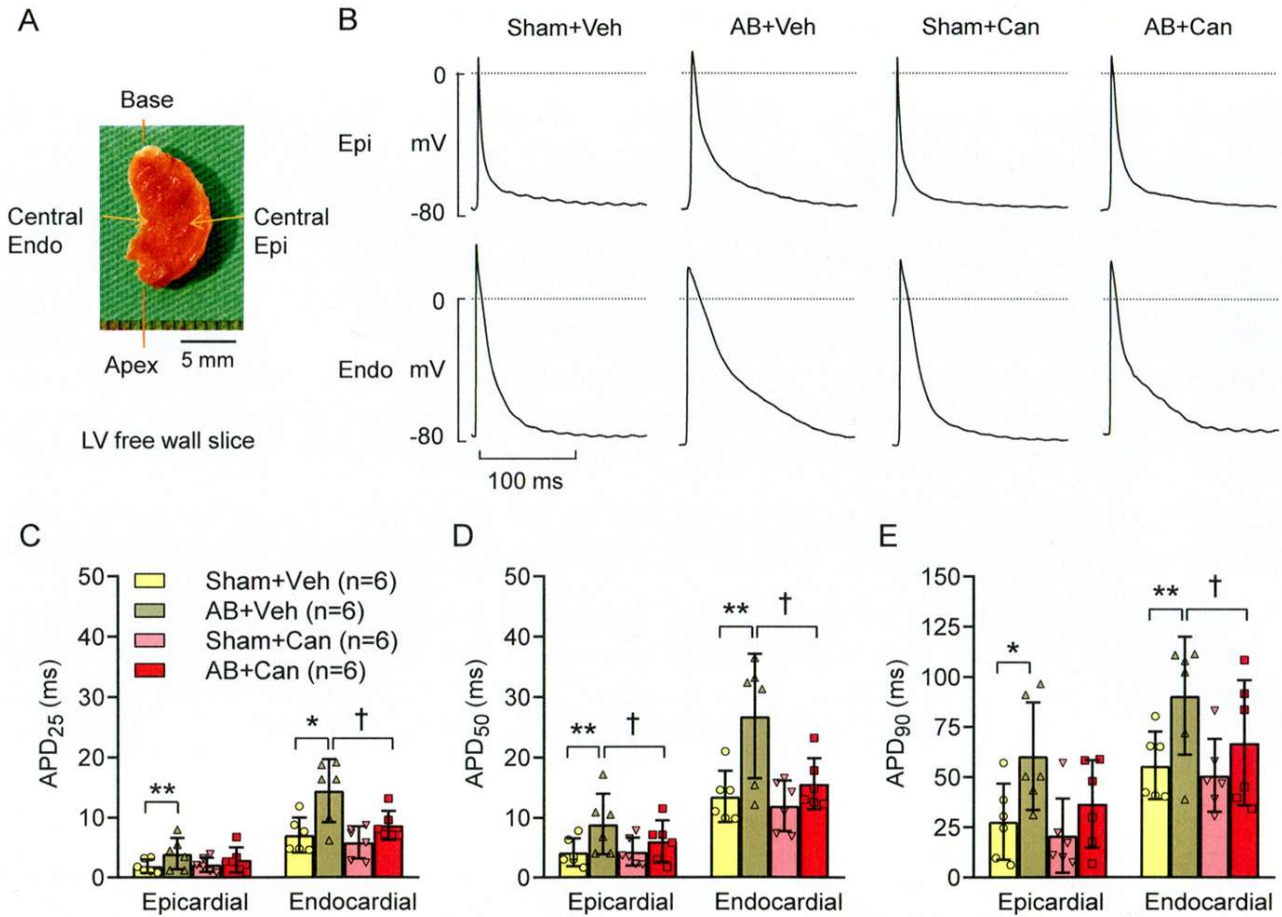
A, Representative images of Masson's trichrome-stained sections ($\times 200$) of left ventricular (LV, upper panel) and left atrial (LA, lower panel) free walls from rats of each group. Collagen (fibrosis) is stained blue. **B** and **C**, Mean interstitial fibrosis area of LV (**B**) and LA (**C**) free walls calculated from sections of Sham (S)+vehicle (Veh) ($n=9$ rats in LV and 8 rats in LA), aortic banding (AB)+Veh ($n=9$ both in LV and LA), S+candesartan cilexetil (Can) ($n=8$ both in LV and LA), and AB+Can ($n=9$ both in LV and LA) groups. Data are presented as means \pm SD. * $P<0.05$ and # $P<0.001$ vs. Sham+Veh group; † $P<0.05$ and ‡ $P<0.01$ vs. AB+Veh group by one-way ANOVA with a Tukey's post hoc test.

Figure S3. Transmembrane action potential variables in left atrial strips isolated from various group hearts.



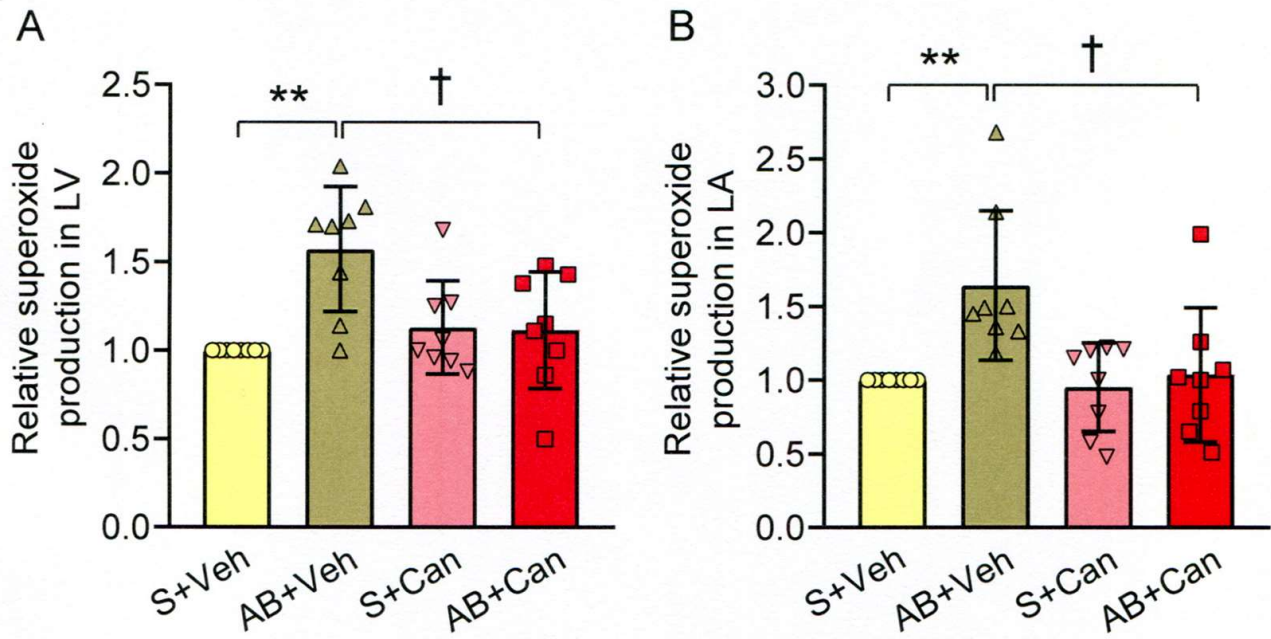
A, Representative superimposed action potential traces obtained from left atrial strips stimulated at 1 or 4 Hz. **B–G**, Effects of increased stimulus frequency (0.5–4 Hz) on action potential duration (APD) at the 25%, 50%, and 90% repolarization levels (APD₂₅, ₅₀, ₉₀), maximal depolarization velocity (dV/dt_{max}), action potential amplitude, or resting membrane potential (RMP) in all groups. Veh indicates vehicle; AB, aortic banding; Can, candesartan cilexetil. Values are presented as means±SD. Data were analyzed by two-way ANOVA.

Figure S4. Transmembrane action potential variables recorded in central subepicardial and subendocardial sites of left ventricular (LV) free wall slices isolated from various group hearts.



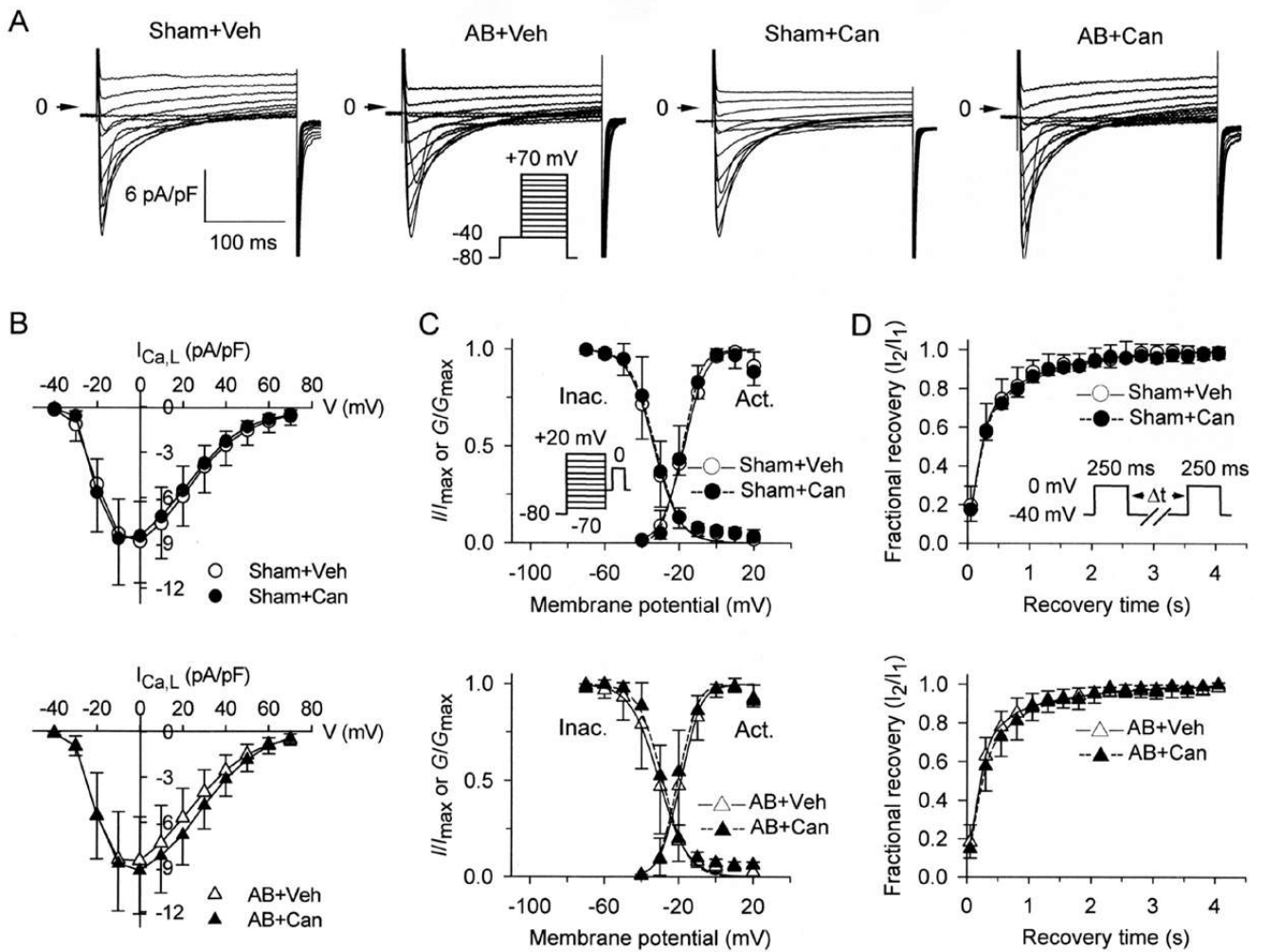
A, Schematic diagram of a LV free wall slice preparation (0.2 mm thickness) isolated from a vehicle-treated banded rat. A microelectrode (arrow) was used to record transmembrane action potential from subepicardial (Epi) or subendocardial (Endo) site. **B**, Representative action potentials obtained from Epi (upper panel) and Endo (lower panel) sites from various group hearts. Stimulus frequency was 1 Hz. **C–E**, Averaged action potential duration (APD) variables at the 25%, 50%, and 90% repolarization levels (APD₂₅, ₅₀, and ₉₀) calculated from subepicardial and subendocardial action potentials in all groups. Veh indicates vehicle; AB, aortic banding; Can, candesartan cilexetil. Values are presented as means±SD. * $P < 0.05$ and ** $P < 0.01$ vs. Sham+Veh group; † $P < 0.05$ vs. AB+Veh group by one-way ANOVA with a Tukey's post hoc test.

Figure S5. NADPH-dependent superoxide anion production in left ventricular (LV) and left atrial (LA) tissues from various group hearts.



Mean value of relative superoxide production of LV (**A**) and LA (**B**) free walls from 8 rats in each group. S indicates sham; Veh, vehicle; AB, aortic banding; Can, candesartan cilexetil. Data are presented as means±SD. Value is expressed relative to Sham+Veh group. ** $P < 0.01$ vs. Sham+Veh group and † $P < 0.05$ vs. AB+Veh group by one-way ANOVA with a Tukey's post hoc test.

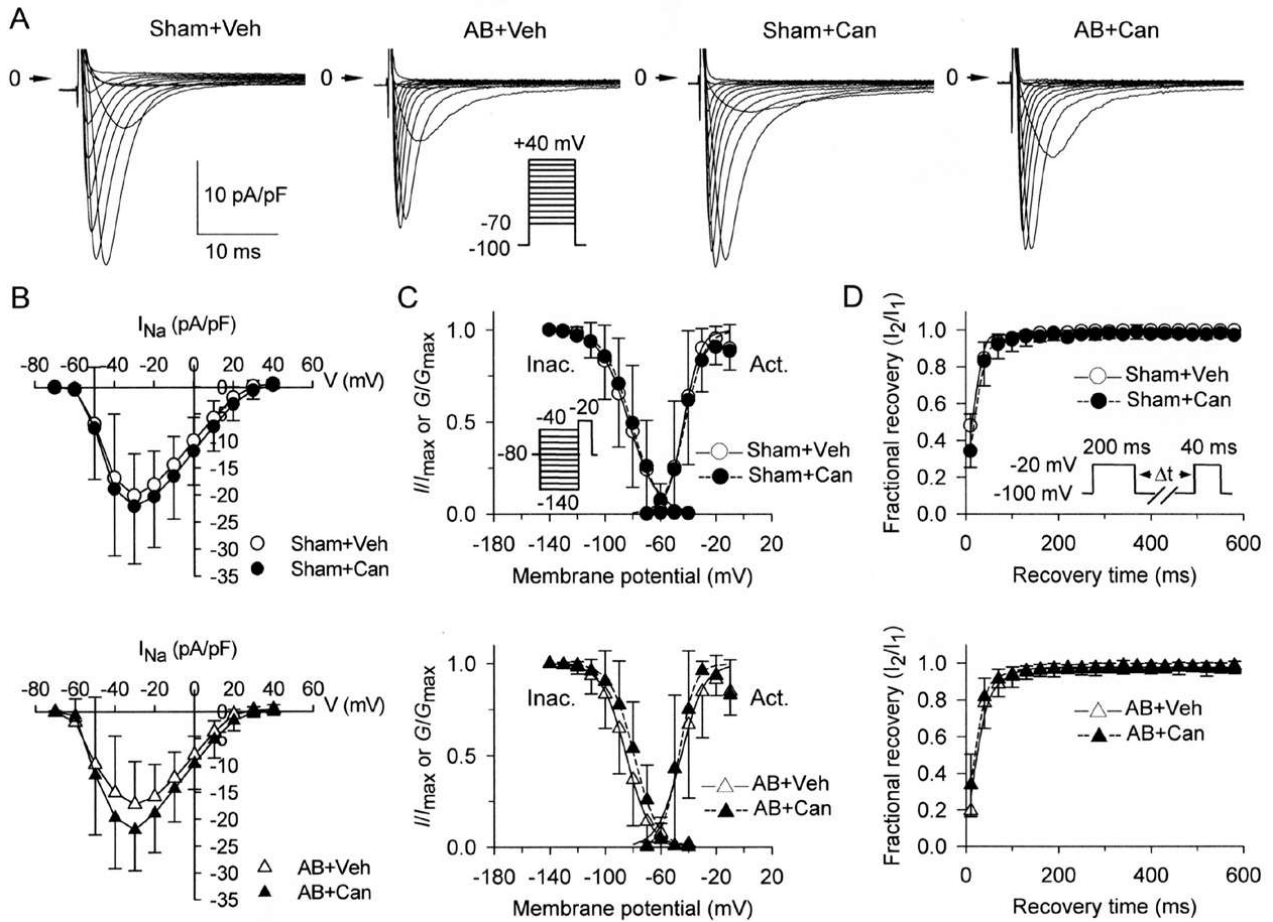
Figure S6. Comparison of L-type Ca^{2+} current ($I_{\text{Ca,L}}$) among various groups.



A, Sample current tracings obtained in left ventricular (LV) myocytes from Sham+Veh (194 pF), Sham+Can (174 pF), AB+Veh (306 pF), and AB+Can (268 pF) groups. $I_{\text{Ca,L}}$ traces were elicited by applying a series of 250-ms long step pulses between -40 and $+70$ mV from a holding potential of -80 mV, after a prepulse to -40 mV to inactivate I_{Na} and T-type Ca^{2+} current. Veh indicates vehicle; AB, aortic banding; Can, candesartan cilexetil. **B**, Averaged $I-V$ relationships of $I_{\text{Ca,L}}$ in myocytes from various group rats. The amplitude of $I_{\text{Ca,L}}$ was measured as the difference between the peak current and the current at the end of the pulse. Each data point represents means \pm SD from Sham+Veh ($n=10$ cells/4 rats; $C_m=204\pm 44$ pF), Sham+Can ($n=10/5$; $C_m=242\pm 58$ pF), AB+Veh ($n=11/4$; $C_m=304\pm 65$ pF), and AB+Can ($n=10/4$; $C_m=262\pm 32$ pF) rats. **C**, Voltage dependence of activation (Act.) and steady-state inactivation (Inac.) of $I_{\text{Ca,L}}$ from various group myocytes. The activation curves were derived using $I-V$ curves shown in panel **B**. Steady-state inactivation was examined with a

double pulse protocol (inset): 1-s conditioning pulses were applied in 10 mV steps between -70 mV and $+20$ mV from a holding potential of -80 mV, and then the test pulse of 200-ms duration was applied to 0 mV (interpulse duration was 30 ms). Line curves shown are fits of mean data by Boltzmann distribution. Each point is the means \pm SD from individual group cells. The number of myocytes/rats used for activation and inactivation studies are 10/5 and 9/4, 10/4 and 9/4, 11/5 and 10/4, and 10/4 and 10/4, respectively, in Sham+Veh, Sham+Can, AB+Veh, and AB+Can rats. **D**, Time course of recovery from inactivation of $I_{Ca,L}$ in myocytes from Sham+Veh (n=9 cells/4 rats), Sham+Can (n=8/4), AB+Veh (n=9/4), and AB+Can (n=11/5) group rats. Recovery was determined with the paired-pulse protocol as shown in the inset. The normalized recovery fraction of $I_{Ca,L}$ ($I_{\text{test pulse}}/I_{\text{prepulse}}$) was plotted against the recovery times. Each curve was adequately fit by a bi-exponential function. Data were analyzed by linear mixed model analysis.

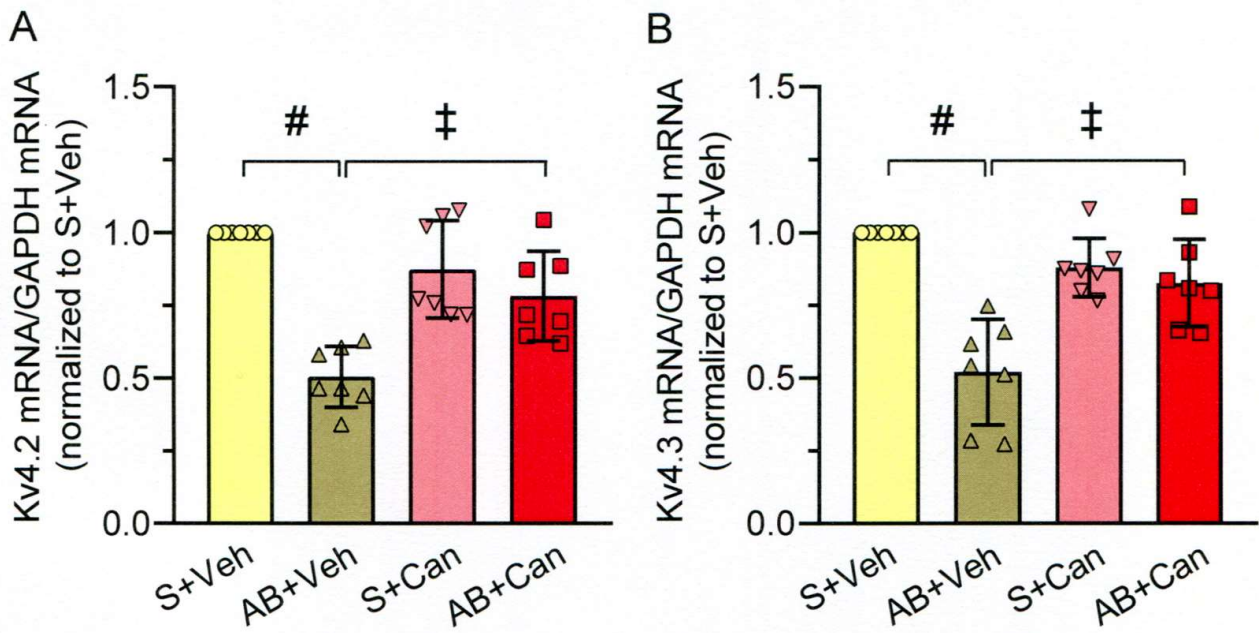
Figure S7. Comparison of peak Na⁺ current (I_{Na}) among various groups.



A, Sample current tracings obtained in left ventricular (LV) myocytes from Sham+Veh (160 pF), Sham+Can (173 pF), AB+Veh (249 pF), and AB+Can (209 pF) groups. Peak I_{Na} traces were evoked by applying the depolarizing steps to test potentials ranging between -70 and +40 mV (10-mV steps, 30-ms duration) from a holding potential of -100 mV. Veh indicates vehicle; AB, aortic banding; Can, candesartan cilexetil. **B**, Averaged $I-V$ relationships of peak I_{Na} in myocytes from various group rats. The amplitude of peak I_{Na} was measured as the difference between the peak current and the current at the end of the pulse. **C**, Voltage dependence of activation (Act.) and steady-state inactivation (Inac.) of peak I_{Na} from various group myocytes. The activation curves were derived using $I-V$ curves shown in panel **B**. Steady-state inactivation of peak I_{Na} was examined with a double-pulse protocol: 1-s conditioning pulses were applied in 10-mV steps between -140 to -40 mV from a holding potential of -80 mV, and then the test pulse of 50-ms duration was applied to -20 mV. Line curves shown are fits of mean data by Boltzmann distribution. Data in panels **B-C** are presented as means \pm SD from

Sham+Veh (n=14 cells/4 rats; $C_m=220\pm 46$ pF), Sham+Can (n=12/4; $C_m=196\pm 56$ pF), AB+Veh (n=16/6; $C_m=258\pm 72$ pF), and AB+Can (n=12/5; $C_m=234\pm 95$ pF) rats. **D**, Time course of recovery from inactivation of peak I_{Na} in myocytes from Sham+Veh (n=12 cells/4 rats), Sham+Can (n=11/4), AB+Veh (n=14/5), and AB+Can (n=11/5) rats. Recovery was determined with the paired-pulse protocol as shown in the inset. A 50-ms prepulse was first applied from a holding potential of -100 mV to -20 mV, which was followed by a 20 ms test pulse after variable interpulse intervals ranging from 10 to 580 ms. The normalized recovery fraction of peak I_{Na} ($I_{test\ pulse}/I_{prepulse}$) was plotted against the recovery times. Each curve was adequately fit by a monoexponential function. Data were analyzed by linear mixed model analysis.

Figure S8. Expression of mRNAs for Kv4.2 and Kv4.3 in left ventricular (LV) tissues from various group hearts.



Bars represent means \pm SD of relative mRNA of Kv4.2 (**A**) and Kv4.3 (**B**) in LV tissues from 7 rats in each group. All measurements were normalized to the levels of GAPDH. S indicates sham; Veh, vehicle; AB, aortic banding; Can, candesartan cilexetil. Value is expressed relative to Sham+Veh group. # $P < 0.001$ vs. Sham+Veh group and ‡ $P < 0.01$ vs. AB+Veh group by one-way ANOVA with a Tukey's post hoc test.